UMEÅ UNIVERSITY

# Blood flow assessment in cerebral arteries with 4D flow magnetic resonance imaging

## An automatic atlas-based approach

Tora Dunås

Department of Radiation Sciences
Department of Pharmacology and Clinical Neuroscience
Umeå 2017

Dissertation for PhD
ISBN: 978-91-7601-889-7
ISSN: 0346-6612
New series No. 1965
Cover image reprinted from: A Stereotactic Probabilistic Atlas for the Major Cerebral Arteries, *Neuroinformatics,* 15(1):101–110, 2017.
Electronic version available at: http://umu.diva-portal.org/
Printed by: UmU Print Service, Umeå University
Umeå, Sweden 2018

*Buy an atlas and keep it by the bed*
*Remember you can go anywhere*

- *Joanna Lumley*

# Abstract

**Background:** Disturbed blood flow to the brain has been associated with several neurological diseases, from stroke and vascular diseases to Alzheimer's and cognitive decline. To determine the cerebral arterial blood flow distribution, measurements are needed in both distal and proximal arteries.

4D flow MRI makes it possible to obtain blood flow velocities from a volume covering the entire brain in one single scan. This facilitates more extensive flow investigations, since flow rate assessment in specific arteries can be done during post-processing. The flow rate assessment is still rather laborious and time consuming, especially if the number of arteries of interest is high. In addition, the quality of the measurements relies heavily on the expertise of the investigator.

The aim of this thesis was to develop and evaluate an automatic post-processing tool for 4D flow MRI that identifies the main cerebral arteries and calculates their blood flow rate with minimal manual input. Atlas-based labeling of brain tissue is common in toolboxes for analysis of neuroimaging-data, and we hypothesized that a similar approach would be suitable for arterial labeling. We also wanted to investigate how to best separate the arterial lumen from background for calculation of blood flow.

**Methods:** An automatic atlas-based arterial identification method (AAIM) for flow assessment was developed. With atlas-based labeling, voxels are labeled based on their spatial location in MNI-space, a stereotactic coordinate system commonly used for neuroimaging analysis. To evaluate the feasibility of this approach, a probabilistic atlas was created from a set of angiographic images derived from 4D flow MRI. Included arteries were the anterior (ACA), middle (MCA) and posterior (PCA) cerebral arteries, as well as the internal carotid (ICA), vertebral (VA), basilar (BA) and posterior communicating (PCoA) arteries. To identify the arteries in an angiographic image, a vascular skeleton where each branch represented an arterial segment was extracted and labeled according to the atlas. Labeling accuracy of the AAIM was evaluated by visual inspection.

Next, the labeling method was adapted for flow measurements by pre-defining desired regions within the atlas. Automatic flow measurements were then compared to measurements at manually identified locations. During the development process, arterial identification was evaluated on four patient cohorts, with and without vascular disease. Finally, three methods for flow quantification using 4D flow MRI: k-means clustering; global thresholding; and local thresholding, were evaluated against a standard reference method.

**Results:** The labeling accuracy on group level was between 96% and 87% for all studies, and close to 100% for ICA and BA. Short arteries (PCoA) and arteries with large individual anatomical variation (VA) were the most challenging. Blood flow measurements at automatically identified locations were highly correlated (r=0.99) with manually positioned measurements, and difference in mean flow was negligible.

Both global and local thresholding out-performed k-means clustering, since the threshold value could be optimized to produce a mean difference of zero compared to reference. The local thresholding had the best concordance with the reference method (p=0.009, F-test) and was the only method that did not have a significant correlation between flow difference and flow rate. In summary, with a local threshold of 20%, ICC was 0.97 and the flow rate difference was -0.04 ± 15.1 ml/min, n=308.

**Conclusion:** This thesis work demonstrated that atlas-based labeling was suitable for identification of cerebral arteries, enabling automated processing and flow assessment in 4D flow MRI. Furthermore, the proposed flow rate quantification algorithm reduced some of the most important shortcomings associated with previous methods. This new platform for automatic 4D flow MRI data analysis fills a gap needed for efficient in vivo investigations of arterial blood flow distribution to the entire vascular tree of the brain, and should have important applications to practical use in neurological diseases.

# Table of Contents

# Original papers

This thesis is based on the following papers, which are referred to by their Roman numerals in the text:

I. **Dunås, T**., Wåhlin, A., Ambarki, K., Zarrinkoob, L., Birgander, R., Malm, J., Eklund, A. (2016) Automatic labeling of cerebral arteries in magnetic resonance angiography. *Magnetic Resonance Materials in Physics, Biology and Medicine*, vol. 29, no. 1, pp. 39–47.*

II. **Dunås, T**., Wåhlin, A., Ambarki, K., Zarrinkoob, L., Malm, J., Eklund, A. (2017) A Stereotactic Probabilistic Atlas for the Major Cerebral Arteries. *Neuroinformatics*, vol. 15, no. 1, pp. 101–110.*

III. **Dunås, T**., Wåhlin, A., Zarrinkoob, L., Malm, J., Eklund, A. 4D flow MRI - Automatic assessment of blood flow in cerebral arteries. *In manuscript*.

IV. **Dunås T.**,** Holmgren M.**, Wåhlin A., Malm J., Eklund A., Blood flow assessment in cerebral arteries with 4D flow MRI, concordance with 2D PCMRI. *In manuscript*.

*Reprinted with permission

** TD and MH contributed equally to the work

# Abbreviations

| | |
|---|---|
| AAIM | Automatic atlas-based arterial identification method |
| ACA | Anterior cerebral artery |
| ACoA | Anterior communicating artery |
| AVR | Arterial volume ratio |
| BA | Basilar artery |
| CD | Complex difference images |
| CoW | Circle of Willis |
| CT | Computed tomography |
| CTA | Computed tomography angiography |
| DARTEL | Diffeomorphic Anatomical Registration Through Exponentiated Lie algebra |
| DSA | Digital subtraction angiography |
| FRQ | Flow rate quantification method |
| ICA | Internal carotid arteries |
| ICC | Intraclass correlation |
| MCA | Middle cerebral artery |
| MNI | Montreal Neurological Institute |
| MRA | Magnetic resonance angiography |
| MRI | Magnetic resonance imaging |
| PCA | Posterior cerebral arteries |
| PCMRI | Phase-contrast magnetic resonance imaging |
| PCoA | Posterior communicating arteries |
| PCVIPR | Phase Contrast Vastly under-sampled Isotropic PRojection imaging |
| RF-pulse | Radio frequency pulse |
| SNR | Signal-to-noise ratio |
| SPM | Statistical Parametric Mapping |
| TCD | Transcranial Doppler |
| TIA | Transient ischemic attack |
| tMIP | Time maximum intensity projection |
| TOF | Time of flight MRA |
| UBA167 | Umeå Brain Arteries - Atlas based on 167 subjects |
| UBA24 | Umeå Brain Arteries - Atlas based on 24 subjects |
| VA | Vertebral arteries |
| Venc | Velocity encoding |
| VNR | Velocity-to-noise ratio |

# Introduction

Assessment of blood flow in the cerebral arteries is challenging but important. Vascular disease is a major cause of impairment and death in the population[1]. Blood flow disturbances have been shown to impact both risk and outcome of ischemic stroke and other neurological diseases such as Alzheimer's and vascular dementia[2–7].

In ischemic stroke, the blood flow to the brain is compromised due to a stenosis or occlusion of a cerebral artery. Sometimes, alternative pathways can be activated so that the blood reaches the affected area despite the obstruction. These paths are called collateral pathways, and their extent varies between individuals[8,9]. Therefore, blood flow measurements in connection to the stenosis do not tell the whole story, and blood flow measurements in more distal arteries, supplying the affected part of the brain, can help fill the gaps.

One way to access blood flow rates throughout the whole arterial cerebral circulation is with 4D flow MRI[10,11] a technique where blood flow velocity can be obtained in a volume covering the whole brain with sub-millimeter isotropic resolution in less than ten minutes.

To fully utilize the properties of 4D flow MRI, advanced post-processing tools are needed. Today most 4D flow MRI analyses are done with manual or semi-manual methods[12,13], which can be time consuming when looking at many arteries. By automating this process, radiologists can focus on interpreting flow values rather than producing them.

For such automatic tools to be useful, they need to identify the arteries of interest and quantify their flow rate. Atlas-based labeling is commonly used for labeling of brain tissue[14,15], but has not yet been evaluated for arterial labeling. Some methods for automatic vessel segmentation and flow quantification have been presented[16,17], but in contrast to the heart and aorta[18] there is no consensus on how to analyze 4D flow MRI of cerebral arteries.

In this thesis, an automatic tool for identifying cerebral arteries and measuring their blood flow rate is presented and validated. This method is based on a large stereotactic probabilistic atlas, constructed from manually labeled 4D flow MRI angiograms.

# Background

## Cerebral arteries and collateral circulation

The brain is supplied with blood through the internal carotid arteries (ICA) and vertebral arteries (VA) (Figure 1). Inside the cranium, the two VA merges to form the basilar artery (BA) which then bifurcates to the left and right posterior cerebral arteries (PCA), while each ICA bifurcates to the anterior (ACA) and middle cerebral artery (MCA). These arteries are then joined together through the anterior (ACoA) and posterior communicating arteries (PCoA) to form the circle of Willis (CoW) (Figure 1).

The CoW functions as a collateral system, which means that blood can be redistributed to compensate for insufficient flow in other arteries. Having a well-functioning collateral system increases the chances of a good outcome of stroke[19]. However, absence or underdevelopment of one or more arterial segment in the CoW is very common[20–22]. A missing ACoA or PCoA will not affect the circulation in the normal situation, but it weakens the collateral function of the CoW (Figure 1). Two common deviations of the CoW are that the pre-ACoA part of ACA (A1), or the pre-PCoA part of PCA (P1) is missing; the latter is called a fetal PCA since it is a remainder from the fetal stage. In both these cases, the presence of a functional ACoA or PCoA respectively is crucial for maintained circulation. The VAs are not considered part of the CoW, but deviations in their anatomy do affect the collateral function. The relative size of the two VAs varies a lot within the population, where in most cases the left VA is larger than the right one[23,24].

The CoW is the primary collateral system, in addition to this there are secondary collateral systems, such as the leptomeningeal and extracranial collateral circulations[8]. In the leptomeningeal system, different vascular territories are connected through cortical anastomoses, and in the extracranial system, the extracranial and intracranial circulation is connected through the ophthalmic artery and the arteries of the face. Both these collateral system allows for retrograde flow distal to the stenosis or embolus, to ensure continued blood supply to the affected area[8].

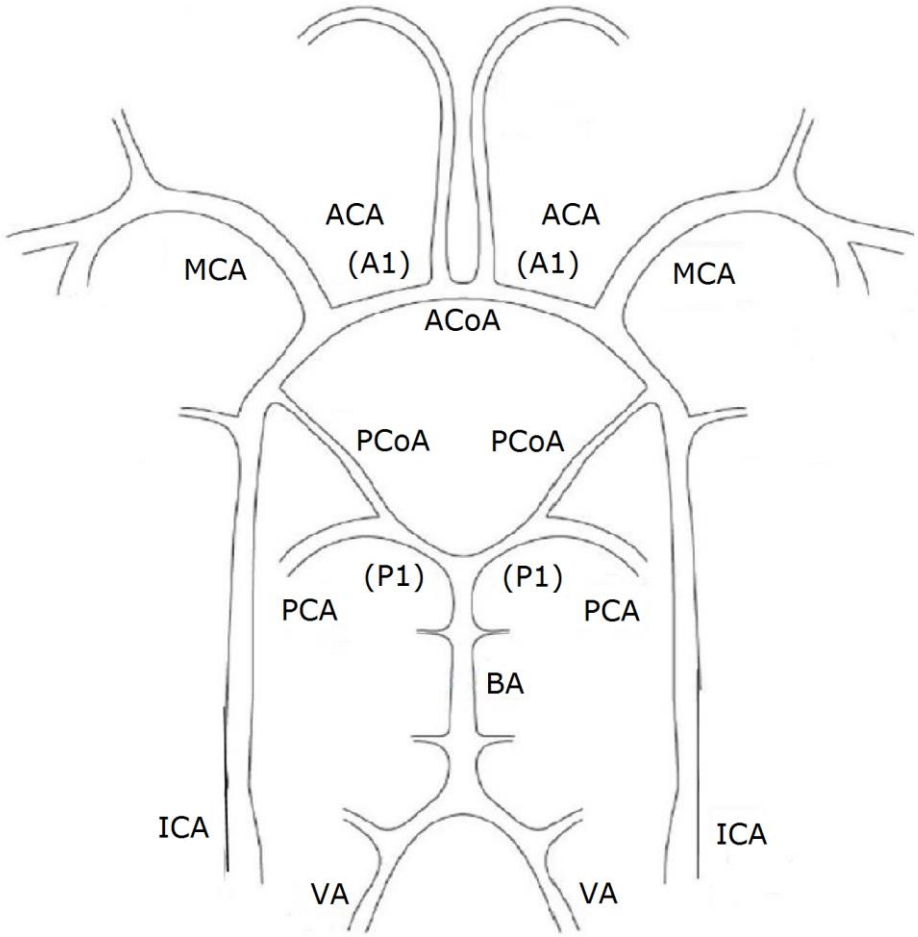


**Figure 1:** *Circle of Willis: Internal carotid arteries (ICA), anterior cerebral arteries (ACA, A1), middle cerebral arteries (MCA), vertebral arteries (VA), basilar artery (BA), posterior cerebral arteries (PCA, P1), anterior communicating artery (ACoA) and posterior communicating arteries (PCoA).*

## Stroke

A stroke can be either ischemic (80%) or hemorrhagic (20%)[25]. Hemorrhagic stroke is caused by a bleeding in the brain, the most common etiologies are hypertension or aneurysms[26].

Ischemic stroke can be defined as a lack of oxygen and energy depletion in the brain tissue, caused by impaired blood flow. There are three main causes for ischemic stroke: 1. Cardioembolic disease, where a blood clot is formed in the heart and travels up to the brain[26]. 2. Atherosclerosis (large vessel disease), where plaque builds up in the extracranial or large intracranial arteries to form a stenosis or occlusion[26]. This can either cause an obstruction at the location, disturb the flow pattern causing blood to coagulate and form a cloth (thrombus), or the plaque can burst and cause an embolus that travels with the blood flow, and causes a blockage further out in the vascular system. 3. Small vessel disease, caused by stenosis or occlusion of small end arteries, which generally results in lacunar infarcts, lesions in subcortical tissue with a diameter under 15 mm[25,26]. A type of small vessel disease is white matter lesions or white matter hyper intensities, named for their appearance on magnetic resonance imaging (MRI). They typically occur with age and usually do not cause any acute symptoms, but a larger size and/or number have been connected to low cerebral blood flow and high pulsatility, as well as cognitive decline[27]. An emboli or thrombosis can also cause a transient ischemic attack (TIA), a temporary reduction of blood flow to the brain or eye[28]. The risk of a stroke occurring after a TIA is high in both the long and the short term[29,30], therefore a TIA should be taken seriously, even though the symptoms disappears.

## Angiography

Angiography is used to visualize the vasculature to find vascular malformations or obstructions of the blood flow. Digital subtraction angiography (DSA) is considered the golden standard for cerebral angiography, but is more and more often replaced by computed tomography angiography (CTA) or MR-angiography (MRA)[31]. Both DSA and CTA require injection of a contrast agent, which can be damaging for the kidneys[32], while MRA can be done both with and without contrast enhancement. In DSA, the contrast agent is administered through catheters inserted into the major arteries, which is not needed for CTA and MRA contrast agents. DSA is therefore considered to be more invasive and is associated with more complications[33,34].

The most common non-contrast enhanced MRA-technique is time of flight (TOF) MRA, where the static tissue is magnetically saturated using repeated excitations. When fresh, non-saturated blood flows in to the imaging volume, it will have a much stronger signal compared to the background, and can therefore be imaged[31].

## Magnetic resonance imaging

An advantage of MRI compared to other radiologic methods is that no ionizing radiation is used; instead MRI utilizes interactions between atomic nuclei, and uses external magnetic fields to form images. Generally, hydrogen nuclei are imaged due to their abundance in the body through water and fat[35]. The property of the nuclei that is used for imaging is called spin, and can be regarded as a rotation around an arbitrary axis. When an external magnetic field ($B_0$) is applied, the spins start to rotate around the direction of that field as well, producing a net magnetization of the tissue in the direction of the $B_0$ field[36]. The frequency of this rotation is called the Larmor frequency, and is proportional to the strength of the external magnetic field.

A second perpendicular magnetic field ($B_1$) oscillating with the Larmor frequency is used to excite the spins, pushing the net magnetization away from the $B_0$ direction, towards the transverse plane. The shift induced by this so-called radio frequency (RF)-pulse is called the flip angle and is dependent on the duration of the RF-pulse[36]. When the spins rotate within the magnetic field, an electric current, proportional to the magnetic moment, is induced in the receiver coils in the MR camera[35]. When the $B_1$ field is removed, the spins start to return to their original state, i.e. aligned with $B_0$, a process known as relaxation. The most energy effective direction of the spin is aligned with the $B_0$ field, therefore the spins tend to fall back into that state, causing a gradual build-up of magnetization; this is called longitudinal (T1) relaxation[35]. Different tissues have different T1 relaxation time, which is defined as the time it takes to build up 63% of the original energy after a 90° flip. At a $B_0$ field strength of 3T, T1 relaxation time for blood is about 1550-2000 ms[37–39], for grey matter about 1100-1700 ms and for white matter about 800-1100 ms[40].

To form an image, spatial encoding is needed to arrange the signals based on their location in the imaging volume. This is done by adding gradient fields which alter the magnetic field, and hence the Larmor frequency, over the volume. This process is based on the physical principle that spins in a stronger magnetic field rotate quicker, i.e. have a higher frequency, than those a weaker field. If this is done during the excitation step, only the slice where the spins have a Larmor frequency corresponding to the frequency of the radiofrequency RF-pulse will be excited, selecting this specific slice which can then be imaged[36]. To encode the two remaining directions, phase- and frequency-encoding is used. By adding a gradient in one of these directions during readout (the readout direction), the placement can be determined based on the frequency of the spins. By briefly applying a gradient in the other of these directions (the phase encoding direction) before readout, the rotation frequency of the spins will change, leaving a phase shift when the gradient is turned off. This must be repeated for each row in the image, with a new excitation and readout in between[36]. This data is then saved in a matrix called k-space, where each row corresponds to one read out, and each point corresponds to one specific frequency and phase. From this data, the image can be reconstructed using mathematical operations, in most cases using inverse discrete Fourier transforms[36].

To image a whole volume rather than just a single slice, the above described process can either be repeated over multiple slices, or data can be collected in 3D by exciting a whole slab and adding a second phase encoding gradient. This gradient is then stepped through in the same way as the first phase encoding gradient[36]. This will of course increase the imaging time accordingly, but there are ways to get around this, for example by squeezing several read-outs into the same excitation, or reducing the waiting time between excitations by using a smaller flip angel and hence depositing less energy[36,41]. Another common way to shorten the imaging time is to use parallel imaging, where information from several coils is combined to form the image, making it possible to compensate for under sampling[36,42]. In MRI, there is always a tradeoff between imaging time, resolution, and signal-to-noise ratio (SNR). By increasing the $B_0$ field strength,

the SNR is increased, making it possible to increase image resolution without compromising quality or imaging time[43].

## Phase contrast MRI

Intracranial blood flow velocity is commonly measured with either ultrasound, such as transcranial Doppler (TCD)[44], or 2D phase-contrast (PC) MRI[45]. The acoustic properties of the scull are not suitable for ultrasound measurements, and blood flow in intracranial arteries can therefore only be measured at specific locations, through openings or thin parts of the cranium. In up to 11% of subjects, the cranium is too thick to obtain TCD measurements[46].

In 2D PCMRI, a phase shift is induced in the spins, proportional to their velocity, using a bipolar gradient field. A bipolar gradient is a magnetic field with two lobes with equal area and opposite polarity (Figure 2). This gradient will induce a phase shift proportional to the local field strength. For stationary spins, the shift from the positive and negative lobes will cancel each other, but moving spins will experience different field strength during the positive and negative lobe, and there will be a residual phase shift. A fast-moving spin will travel further along the gradient, resulting in a larger difference between the positive and negative field strength, and hence a larger residual phase shift (Figure 2)[36]. When collecting PCMRI data, a specific encoding velocity (Venc) is specified; this is the velocity corresponding to a phase shift of 180 degrees. Velocities exceeding this limit will be interpreted as negative, since a phase shift of 180 + α cannot be distinguished from -180 + α, this error is called aliasing. It is important to select a suitable Venc value, since a too high value will result in a decreased velocity-to-noise ratio (VNR)[11], which is proportional to the ratio between SNR and Venc[47].

In 2D PCMRI, only one velocity encoding direction is used, placing a measurement plane perpendicular to the desired flow direction specifies this direction. During the last decade, a new set of techniques called 4D flow MRI[11,48], has emerged. In 4D flow MRI, flow is measured in all three spatial directions, covering a volume instead of a single plane. Both 4D flow MRI and 2D PC MRI

can be time-resolved over the cardiac cycle, giving the fourth dimension in 4D flow MRI.

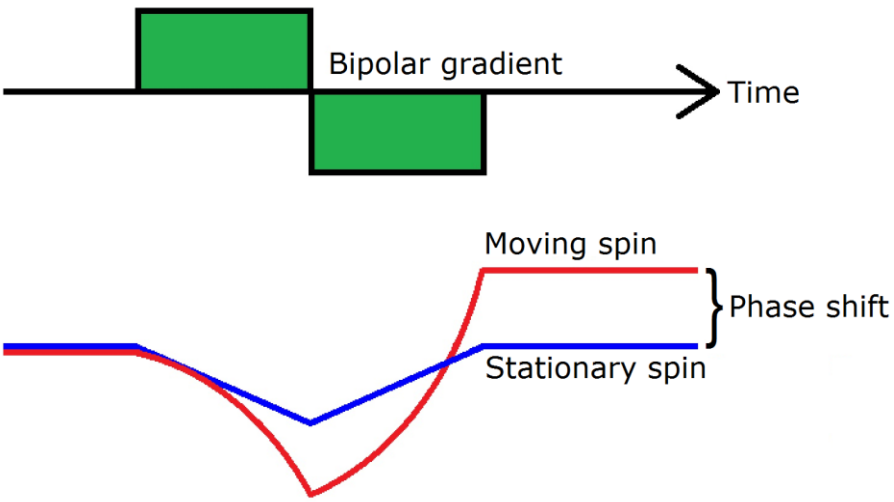


**Figure 2:** *Velocity encoding in phase contrast MRI. A bipolar gradient is applied, inducing a phase shift in moving spins*

Simply extrapolating the technique used in 2D PCMRI to three dimensions would result in extremely long scan times, especially when covering a large volume such as the whole brain. In general, 4D flow MRI sequences are therefore under-sampled. This does not mean that some areas are left uninvestigated; instead assumptions of the underlying image are utilized to optimize data collection and reconstruction. The 4D flow MRI sequences used in this thesis (PCVIPR - Phase Contrast Vastly under-sampled Isotropic PRojection imaging) uses radial under-sampling[10], where radial spokes through the center of k-space are collected. This results in a high sampling-rate at the center of k-space where low frequency contrast information for the tissues is stored, and lower sampling at the edges where high frequencies (sharp edges) are stored. Isotropic imaging means that the image has the same spatial resolution in all directions. There are other 4D flow MRI methods besides PCVIPR[49], for example sequences using spiral sampling[50] or other parallel imaging[51] to reduce scan time.

In addition to neurovascular imaging[52,53], 4D flow MRI is primarily used for investigating various cardiovascular diseases, by imaging of for example the heart[54] or liver[55]. It is also very useful for visualization of flow patterns[56–58] and investigation of flow patterns in aneurysms, which are abnormal dilations of an artery, usually located at an arterial bifurcation[59,60]. From 4D flow MRI data, various hemodynamic parameters can be calculated, such as mean blood flow, pulsatility index[61], wall shear stress and pulse wave velocity[52].

## Image normalization

In neuroimaging, normalization to a stereotactic standardized coordinate system is crucial for comparisons between subjects. Today the most widely used standard coordinate system is MNI (Montreal Neurological Institute) space[62]. The MNI standard brain has been updated several times to improve quality. The MNI atlas implemented in brain mapping software such as SPM (Statistical Parametric Mapping) is the MNI152, where high resolution scans with improved brain coverage from 152 subjects were linearly registered to the earlier MNI305 brain[62].

SPM is a software package for analysis of neuroimaging data[14]. SPM can be used for a variety of image segmentation, registration and normalization processes with different levels of complexity. When aligning different images from the same subject, linear transformations such as scaling and translations might be enough, but when creating averages over subjects, more powerful methods are needed. When choosing a suitable normalization method, it is important to consider what properties of the image that are preserved, especially if calculations are done after normalization. One of the more powerful normalization techniques is DARTEL (Diffeomorphic Anatomical Registration Through Exponentiated Lie algebra)[63], where the transformation between subject and template is calculated by solving a number of partial differential equations.

## Anatomical atlases

An anatomical atlas is a collection of maps containing information that can be used to classify data and make outcome predictions[64] or to enhance anatomical

knowledge about different structures[65,66]. Some vascular atlases contain detailed descriptions of cerebral arteries[67], characterizations of the main arterial trees[68] or describe average vascular density throughout the cerebral space[69], which can be useful for understanding pathologic processes of the cerebrovascular system[70].

Probabilistic atlases are used for tissue segmentation[71], both for specific cerebral regions[15] and other anatomical structures[72], for example the tissue segmentation method used for normalization in SPM[14]. Atlas-based approaches have also been used for vascular segmentation[73], as well as for quantification of blood flow in large thoracic vessels[74], and information on spatial location and branching patterns have been used to identify specific arteries[75–77], but no artery specific probabilistic atlas has yet been proposed.

## Vascular segmentation

An important part of data processing for angiographic images is the separation of vessels from the background. The complexity of this problem depends largely on imaging objective and type of image[78,79]. With a good angiographic image, a simple thresholding could be enough to separate vessel from background, especially if the main interest is larger arteries[50]; thresholding could also be used as a first step to remove background before more advanced segmentation methods are applied[80]. More advanced statistical methods[81,82] or methods incorporating a priori knowledge[83] can also be employed. There are also centerline based methods where a vascular centerline is first detected, and the 3D rendering of the vascular tree is then recreated by cross-section calculations or fittings at each point along the centerline[84].

If the main interest is to calculate flow rates or other flow parameters at a specific location, a coarse segmentation can be used to detect the arteries. A 2D cross-section through the selected artery can then be calculated and a more advanced method can be applied to refine the segmentation within this plane. In this case, manual segmenting is common[85,86] sometimes in combination with automated fitting[13], but thresholding can also be used, either at a fixed level[16] or manually adjusted for each case[87], as well as clustering[17] or more advanced analysis of flow

patterns[88]. With a segmentation of a cross-section plane, the approach is very similar to the segmentation challenge of 2D PCMRI, where partial volume errors and Gibbs ringing have been shown to affect the flow estimation[89–91]. Also in this case, manual[45,92] or semi-manual[93,94] segmentation is most common, but there are some fully automatic methods that identify the vessel border based on image properties[95,96].

## Automated processing

As methods for data collection get increasingly effective, more and more output data are produced, putting additional pressure on the post-processing and interpretation of that data. More and more studies are also conducted as multicenter studies[97–99], leading to an even larger amount of data as well as a need for standardized methods to ensure good agreement between analyses conducted at different locations and by different investigators.

Automatic processing of images has several advantages such as reduced manual workload and more standardized and reproducible results. Automated methods have been developed for everything from detection of white matter hyperintensities[100] to nerve segmentation[101] and motion corrections[102], in addition to previously mentioned atlas and segmentation methods. For analyses of 4D flow MRI data in cerebral arteries, automated methods are lacking.

# Aim

The main goal of this thesis was to develop a fully automatic post-processing tool for analysis of 4D flow MRI of the main cerebral arteries that locates and labels specific arterial segments and quantifies the blood flow rate in those segments.

More specifically, we wanted to investigate the potential of an atlas-based approach for arterial labeling, and evaluate the suggested methods on subjects with vascular diseases. We also wanted to investigate the reliability of flow measurements in cerebral arteries in 4D flow MRI, using automated vessel segmentation.

Specific aims for the studies were:

I. To propose a method for automatic labeling of cerebral arteries in 4D flow MRI.
II. To construct a stereotactic and probabilistic atlas of the main cerebral arteries, based on manually labeled 4D flow MRI angiographies.
III. To adapt the atlas-based automatic labeling method to facilitate flow measurements, and to validate this method against manually placed measurements on a sample of stroke patients.
IV. To determine and optimize the accuracy of in vivo 4D flow MRI blood flow rate assessments in major cerebral arteries, by comparison with 2D PCMRI.

# Material and Methods

## Subjects

The studies in this thesis were based on four cohorts; Table 1 shows an overview of the subjects included in each paper:

1. Subject recruited within the COBRA *(Cognition, Brain and Aging)* study[103]. Exclusion criteria were medical conditions that could alter brain function or cognitive performance, and contraindications to MRI.
2. Patients with TIA or lacunar infarcts. Diagnosis was based on case history, neurological examination and brain MRI examination. CTA did not reveal any stenosis or occlusion of internal carotid, vertebral or basilar arteries, or in the middle, anterior or posterior cerebral arteries.
3. Patients with carotid artery stenosis ≥ 50%. Stroke diagnoses were based on case history, neurological and brain MRI examination, and stenosis grading was done with CTA or ultrasound.
4. Elderly subjects who were recruited for this specific study, but also as a ten year follow up to a previous study at our facility[104]. The only exclusion criteria were contraindications to MRI.

**Table 1:** *Overview of subjects included and data used in each paper*

| Paper | Cohort no. | No. subjects | Male/Female | Age (mean ± SD) |
|---|---|---|---|---|
| I | 1 | 112 (24+21+67) | 65/47 | 65.8 ± 1.2 |
| II | 1 | 167 | 97/40 | 65.8 ± 1.2 |
| II | 2 | 10 | 7/3 | 69.4 ± 7.7 |
| III | 3 | 38 | 27/11 | 72.5 ± 5.7 |
| IV | 4 | 35 | 15/20 | 78.7 ± 5.2 |

### *Ethical considerations*

The regional ethical review board approved all separate studies (Dnr. 2012-57-31M, 2011-440-31M, 2012-396-32M, 2017/253-31) and informed consent was obtained from all participants.

## MRI

All data was collected on a 3 Tesla scanner (Discovery MR 750; GE Healthcare, Milwaukee, WI, USA) with a 32-channel head coil. The 4D flow MRI protocol used in all four studies was a five-point PCVIPR sequence[105] with the following parameters: Venc = 110 cm/s, TR = 6.5 ms, TE = 2.7 ms, flip angle = 8°, bandwidth = 166.67 kHz, 16000 radial projections, acquisition resolution = 300 × 300 × 300, imaging volume = 220 × 220 × 220 $mm^2$, reconstruction matrix size = 320 × 320 × 320 (zero padded interpolation) and voxel size 0.7 × 0.7 × 0.7 $mm^3$.

In Paper IV, flow in the major cerebral vessels was also assessed with 2D PCMRI in addition to 4D flow MRI. Parameters used for collection of 2D PCMRI were: Venc = 60-100 cm/s, TR = 7.6-10.7, TE = 4.1-4.7 ms, flip angle = 15° in plane resolution = 0.35 × 0.35 $mm^2$, slice thickness = 3 mm, matrix size = 512 × 512 voxels, 32 time-resolved images reconstructed. Eight 2D PCMRI-planes were placed in a TOF image:

1. ICA just below the skull base
2. BA just below the superior cerebellar artery
3. Right MCA at M1 level
4. Left MCA at M1 level
5. Right ACA at A1 level
6. Left ACA at A1 level
7. Right PCA at P2 level
8. Left PCA at P2 level

## Data processing

From the 4D flow MRI data, velocity maps in x-, y- and z-directions were reconstructed, as well as angiographic complex difference images (CD) and structural T1-weighted magnitude images. For Paper I and II, time resolved reconstruction was used, calculating all this data for 20 timeframes over the cardiac cycle, as well as mean flow reconstruction, where images are calculated for data from all timeframes combined. In Paper I and II, the angiographic image

used was a time maximum intensity projection (tMIP) calculated from all CD over the 20 timeframes. In Paper III and IV we only used the mean flow reconstruction, and hence we used the mean flow CD.

A crucial part of the data processing was the construction of a vascular skeleton. This process included a coarse segmentation of the CD or tMIP, where vessels are separated from background to produce a binary vessel image. In Paper I and II, vessels were separated from background using a global 18% intensity threshold on the tMIP, adapted to give good vessel coverage without including neighboring static tissue[16]. For Paper III and IV, an adapted threshold based on the distribution of intensity values within the image was used[17]. In both cases, to increase SNR, the image was smoothed with a low-pass box filter with a kernel size of three voxels before thresholding. The binary image was gradually thinned to obtain the vascular skeleton[106], the skeleton was pruned to remove loops and short spurs[107], the vascular tree was divided into branches and junction points, and each branch was assigned a specific identification number. This vascular skeleton extraction was a part of both the automatic identification method (Paper I-III), and the atlas construction (Paper I and II). It was also used in the segmentation methods in Paper IV, but not for the manual measurements in Paper III.

## Automatic arterial identification

In Paper I, an automatic atlas-based arterial identification method (AAIM) was developed, where voxels from the vascular skeleton were assigned to different arteries depending on their position in MNI-space. This method forms the basis for the fully automatic tool for assessment of blood flow distribution in cerebral arteries. Table 2 presents which arteries are labeled in each paper.

**Table 2:** *Overview of arteries investigated in each paper*

| Artery | Paper I | Paper II | Paper III | Paper IV |
|---|---|---|---|---|
| ICA C2 | X | X | X | X |
| ICA C4 | | | X | |
| VA | X | X | X | |
| BA | X | X | X | X |
| PCA P1 | * | * | X | |
| PCA P2 | X | X | X | X |
| PCoA | X | X | X | |
| MCA | X | X | X | X |
| Distal MCA | ** | X | | |
| ACA | X | X | X | X |
| Distal ACA | X | X | | |

* Included in P2, ** Included in MCA

### *Atlas construction*

In Paper I, a stereotactic probabilistic atlas (Umeå brain arteries, UBA24) was constructed from 24 subjects, selected so that all included subjects had bilateral VA connecting to the BA, and a complete CoW, except for PCoA. Since the blood flow in PCoA usually is too low for it to show up on the thresholded tMIP when a functioning P1 is present, a second group of 21 subjects, with one or both PCoA visible in the binary image, was used to form the atlas for this artery.

The UBA24 was developed as a proof of concept atlas, and the concept was further advanced in Paper II by expanding the atlas to include both a larger number of subjects and a wider range of arterial morphologies, creating a new atlas (UBA167) from the whole COBRA cohort.

The first step in creating the stereotactic atlas was to transform all data to MNI-space; this was done with the SPM8 toolbox in MATLAB (Mathworks, MA, USA). Probability maps for white matter, grey matter, and cerebrospinal fluid was calculated from the magnitude image using New Segment from the SPM8 toolbox (http://www.fil.ion.ucl.ac.uk/spm). From these probability maps, transformation fields for each subject were calculated with DARTEL[63], and these flow fields were used to transform the angiographic images to MNI-space, where the atlas construction took place.

For the atlas construction in Paper I and II, binarization and vascular skeleton construction were done after MNI transformation. Arteries of interest were manually selected from a 3D rendering of the binary image, using an in-house MATLAB tool. This tool identified vessels based on their centerline, and the arterial segment corresponding to the selected skeleton branch was recreated by dilating the branch to form a tube with a diameter of fifteen voxels, which was then masked with the binary volume to extract the part corresponding to the selected artery. Several segments could be joined together to form the complete artery. When all arteries of interest in all subjects had been manually labeled, edited and approved, the binary volumes representing each artery were added together and divided by the number of included arteries to form a probability map for each artery.

In Paper III, the atlas was further developed to facilitate flow measurements by defining specific regions for each artery where we wanted to obtain measurements (Figure 4). The placement of these regions is specified in Table 3. The atlas regions were constructed by thresholding the atlas to get a smooth surface, and extracting the vascular skeleton from the image. Within this skeleton, a straight segment corresponding to each of the specified regions was selected. The regions were then defined as the intersection between the atlas and a thirteen voxels thick plane perpendicular to the selected segment. No regions were defined for distal ACA and distal MCA, since they consist of several parallel branches, and therefore were not suitable for this kind of labeling. For PCA, P1 was separated from distal PCA (P2), to prepare for complete characterization of flow dynamics in CoW. In ICA, one intracranial (C4) and one extracranial region (C2) were specified to accommodate comparison to data collected at different locations in the vasculature[48,61].

### *Impact of normalization*

The normalization to MNI-space requires substantial computational resources, therefore we wanted to investigate how much the DARTEL normalization improved the spatial alignment of the arteries, and hence to what extent it contributed to improved compactness of the atlas. This was done by comparing

the UBA167 to an atlas without DARTEL normalization, instead relying on rigid body transformation (Paper II). The labeled arteries were transformed back to their native space and aligned using a rigid-body transform. Since these transformations did not preserve the binary property of the volumes, they were re-binarized using a volume-conserving threshold, before construction of the probability maps as previously described. This atlas was not evaluated for labeling, but compared to the UBA167 in terms of compactness. The main parameters used to evaluate this were the maximal probability value in each probability map and the arterial volume ratio (AVR), calculated as the concatenated volume (total number of non-zero voxels) of each probability map, divided by the average volume of the included arteries. Overlap between arterial probability maps was described in terms of dominating volume, calculated as the percentage of non-zero voxels within each probability map where no other probability map had a higher value.

### *Arterial labeling*

Labeling took place in the native space of the target subject, which means that the atlas (UBA24 or UBA167) was matched to the coordinate system of the subject and not the other way around (Paper I and II). DARTEL was used to calculate a transformation field from the subject to MNI-space, and this field was used inversely to transform the atlas to the coordinate system of the subject.

Next, the vascular skeleton of the subject was extracted, and each skeleton voxel was assigned to the artery with the highest probability at the corresponding location in the atlas. Voxels with a maximum probability of zero for all arteries were discarded. In Paper III, where the labeling procedure was adapted for flow measurements, a second cleanup was done, where skeleton voxels that did not fall within the defined atlas regions were discarded.

Each artery was identified as the longest continuous segment of voxels labeled as the artery in question. Segments shorter that eight voxels were discarded since they were considered too short to provide meaningful information and were often incorrectly labeled. For Paper I and II, voxels were considered continuous if they

were part of the same branch, and junction points were included to join adjacent branches. In Paper III, only branch segments without any gaps or junctions were allowed, to avoid placing the seed point for the flow measurements at a bifurcation, and to make sure all consecutive points were adjacent. The output from the AAIM was a list of identified and labeled centerline segments, as well an image of the corresponding arterial volumes.

### *Evaluation of arterial labeling*

The arterial volume corresponding to a labeled centerline segments was recreated in the same way as for the atlas construction. For Paper I and II, all arterial volumes were combined into a single 3D volume, where each artery was color coded and overlaid on the angiographic or magnitude image stack. For Paper III, the volumes were instead presented as color-coded regions on a rotatable 3D rendering of the binary image (Figure 3).

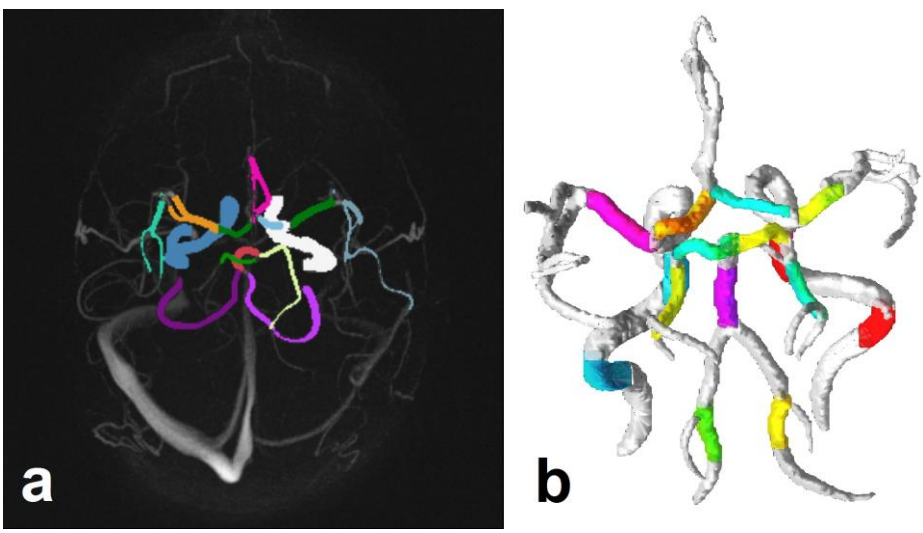


**Figure 3:** *Example of images used for evaluation of labeling in a) Paper I and II, b) Paper III*

Each identified artery was classified as correct or incorrect by visual examination. In Paper I and II, segments could also be labeled as too short if they belonged to the correct artery, but did not fulfill the evaluation length criteria (Table 3). For

Paper III, no length limit except the one implemented in the processing was used. Accuracy, sensitivity and specificity were calculated by comparing these results to a manual reference. If the segment was categorized as incorrect or too short, it was considered a false negative if there was an artery to find, and a false positive if there was not.

**Table 3:** *Evaluation criteria for full artery labeling (Paper I-II) and labeling of specific arterial segments (Paper III)*

| Artery | Paper I-II | Paper III |
|---|---|---|
| ICA C2 | 2 cm cervical segment | Cervical segment (C2) |
| ICA C4 | - | Cavernous segment (C4) |
| VA | 1 cm straight segment in conjunction to the foramen magnum | Anywhere in the artery |
| BA | 1 cm segment anywhere in the artery | Anywhere in the artery |
| PCA P1 | - | Proximal to PCoA or PCoA genu |
| PCA P2 | 1 cm segment distal to PCoA | Distal to PCoA or PCoA genu |
| MCA | 1 cm segment in M1 | Before first bifurcation |
| Distal MCA | 1 cm segment in the sylvian fissure | - |
| ACA | 5 mm segment in A1 | A1 segment |
| Distal ACA | 1 cm segment distal to ACoA | - |
| PCoA | 5 mm segment anywhere in PCoA | Anywhere in the artery |

In Paper I, the existence of arteries was determined based on visual examination of the magnitude image. In Paper II, a leave-one-out-approach was used to validate the UBA167. This means that the data from the target subject was removed from the atlas, and the atlas based on the remaining 166 subjects was used for labeling. The reference for this analysis was based on the manual labeling, arteries were considered present if they were visible in the binary image, and hence were included in the atlas. To do a first preliminary test that the AAIM did not only work on healthy elderly, the AAIM combined with the UBA167 was also evaluated on a small stroke sample, where the manual reference was based on CTA. In Paper III the manual flow measurements functioned as a reference, meaning that the existence of arteries was determined based on the CD.

## Flow quantification

In Paper III, the AAIM was combined with a previously developed flow rate quantification method (FRQ)[16], and the automatic measurements were compared to manually placed measurements, using the same FRQ. In Paper IV, three different approaches to arterial segmentation with a variety of input parameters were evaluated by comparison to flow values obtained by 2D PCMRI.

### *Methods for flow quantification*

The FRQ calculated flow values starting from a seed voxel. The flow direction in this voxel was used to find a three-voxel thick perpendicular plane through the artery, and vessel voxels were separated from background by a global threshold at 10% of the highest intensity value in the CD. The blood flow rate in the artery was calculated as the accumulated flow through all voxels in the plane, within the thresholded region, divided by the thickness of the plane[16].

The methods developed in Paper IV used the local direction of the centerline in a neighborhood of the seed voxel as an approximation of the vessel direction. A volume close to the seed voxel was resampled in the vessel direction, so that a 2D cut-plane perpendicular to the artery could be extracted, and the data within this cut-plane was interpolated to increase the linear spatial resolution with a factor of four.

The segmentation methods evaluated in Paper IV were k-means clustering, global (fixed) thresholding and local (adapted) thresholding. All clustering methods included the CD, either by itself, combined with the magnitude image or the velocity magnitude[17], or with both. In the clustering methods, each input variable was normalized by calculating the z-score, to remove differences in mean and standard deviation between variables and hence give them the same weight.

The thresholding methods were based on the maximum intensity of the CD, either within the whole volume (global threshold), or within the extracted cut-plane (local threshold). Both approaches where evaluated for threshold values ranging from 6% to 26% of the maximum intensity.

All methods evaluated in Paper IV calculated blood flow rate in the same way. The blood flow rate through each voxel in the cut-plane was calculated as the sum of flow velocity in x-, y- and z-direction, multiplied with the corresponding element in the vector describing the direction of the artery and the voxel area. Total flow rate was calculated by summing the flow through each voxel within the segmented area.

### *Evaluation of flow quantification*

In Paper III, automatic measurements of 4D flow MRI were validated against manual measurements on the same data. Two raters performed manual measurements independently by viewing axial images and selecting the seed voxel with the cursor. When the difference between the two measurements exceeded 20% of their mean, a consensus measurement was performed; otherwise the mean of the two measurements was used. For the automatic measurements, the midpoint of the identified centerline segment was used as a seed voxel for flow quantification.

The 2D PCMRI data in Paper IV was processed using Segment (http://segment.heiberg.se)[108], vessels were outlined in the magnitude image and flow rates were calculated. A region of interest (ROI) covering the vessel was manually outlined in the image, considering both the magnitude and the phase image. The ROI size was kept constant through all time frames and flow rate was calculated as the mean value over the 32 timeframes. The spatial information from the 2D PCMRI was translated to the coordinate system of the 4D flow MRI, and the point in the vascular skeleton closest to each of the calculated mid-point of the 2D ROIs were identified and used as a seed point for the 4D flow segmentation. In cases where the closest point was not on the correct branch, the correct branch was manually selected and the closest point on that branch was identified.

Only branches with a length of five voxels or more were used, and seed voxels were placed with a distance of at least two voxels from the ends of the branch. The reason for this was partly to avoid tricky geometries, and partly to investigate if

averaging flow values over several adjacent cut-planes improved SNR. In the main analysis, only values from the midpoint, i.e. the original seed point, were used, but these values were also compared to values averaged over three or five cut-planes based on adjacent seed points.

## Statistics

For all studies that included automatic identification of arteries (Paper I-III), labeling accuracy was calculated as the number of correctly identified existing and correctly identified non-existing arteries, divided by the number of possible arteries. The number of possible arteries includes both the number of existing arteries and the number of arterial segments that are missing anatomically, and we hence do not want to find.

In Paper II, the UBA167 was compared to an atlas without normalization. Since the investigated variables were not normally distributed, non-parametric tests were used. Wilcoxon signed-rank test was used to investigate the difference in AVR and dominating volume between the two atlases, and Spearman correlation was used to investigate the correlation between AVR and labeling accuracy.

In Paper III, two different types of intraclass correlation (ICC) were used to assess agreement between measurements. When comparing results from the two raters to each other, we were not primarily interested in the reliability of these specific raters, and conclusions were made based on the mean values of the two raters rather than the individual measurements, therefore the multiple measurement option (ICC(2,k)) was used[109]. When comparing the automatic measurements to the manual reference, we were specifically interested in the reliability of the automatic measurements compared to the reference, and we used those values separately rather than averaging them, therefore we used the single measurement (ICC(2,1)) option. In Paper IV, we were once again interested of the reliability of the 4D flow measurements compared to the 2D PCMRI, and we therefore used the ICC(2,1). ICC-values with a lower bound of the 95% confidence interval over 0.5 were considered fair, over 0.75 good and over 0.9 excellent, values with a lower bound under 0.5 were considered poor[109].

Agreement between methods was also assessed in terms of mean flow difference, and the statistical significance of such differences was evaluated with a paired t-test, with a significance level set to $p<0.05$. In addition to the mean flow difference, we also wanted to assess the precision of the methods, which was done by calculating the standard deviation of the flow difference between the proposed methods and the reference methods.

In Paper IV, the optimal threshold values for the two thresholding methods was found by minimizing the mean flow difference compared to the reference. The standard deviation of the flow difference was compared between the two methods, with their respective optimal threshold value, and was evaluated with F-tests ($p<0.05$). A suitable segmentation method should not have a flow dependency related to vessel size, which previous experience had shown could be the case. This was investigated using a linear regression of flow difference versus flow rate.

# Results

The main result of this thesis was the construction and evaluation of an atlas-based method for arterial identification and flow measurements.

## Atlas development

A probabilistic cerebral arterial atlas based on 167 individuals (UBA167) was successfully constructed and used for arterial labeling. This atlas consists of 2360 individually segmented and labeled cerebral arteries, divided into 16 probability maps. Within the atlas, 17 regions were defined and validated for flow measurements. The number of arteries on which each of the probability maps is based, varied from the maximum value of 167 (ICA, MCA, distal ACA) down to 30 (left PCoA), with all arteries except PCoA including more than 150 arteries. Figure 4 shows an overview of the different atlases and atlas regions.

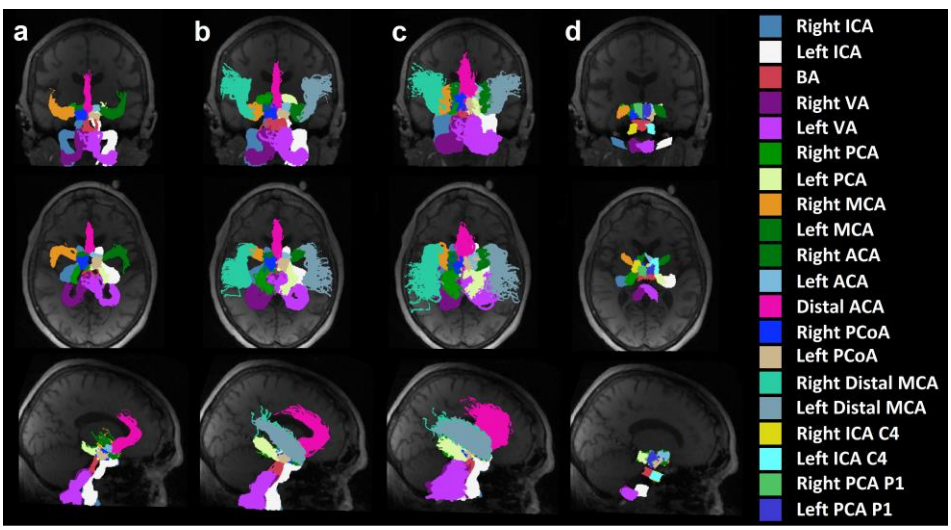


**Figure 4:** *Projection images (top row: coronal, middle row: axial, bottom row: sagittal) of the atlases a) UBA24 (Paper I), b) UBA167 (Paper II), c) Rigid-body atlas (Paper II), d) Atlas regions for flow measurements (Paper III)*

The analysis of spatial alignment showed that the only artery in UBA167 where all subjects overlapped in at least one voxel was ICA. In the atlas based on rigid-body transformation (without normalization), the highest probability value in a

vessel within the atlas was 0.53, and no artery except ICA had a maximum probability value over 0.25. Probability maps corresponding to large proximal arteries had a lower AVR than smaller distal arteries. A low AVR indicates a high agreement between subjects and was correlated to high labeling accuracy. AVR for the whole atlas was more than doubled without the normalization (29.3 compared to 13.7), while dominating volume decreased from 85.8% to 74.9%, both these differences were significant ($p < 0.005$, Wilcoxon signed-rank test).

## Arterial labeling

The accuracy of the arterial labeling was part of the main results for Paper I-III. Accuracy for each arterial group in each of the evaluation groups is presented in Table 4. Overall, the labeling accuracy was high in both healthy subjects and stroke patients. The accuracy on group level was between 96% and 87% for all studies, depending on how the existence of arteries was determined, which arteries were evaluated, and what criteria were used to determine if the labeling was correct or not. Large arteries had consistently higher accuracy than small arteries, for which the results were more affected by study design. The lowest accuracies were found in VA, P1, PCoA and distal MCA, where a variation in morphology between subjects was largest.

**Table 4:** *Labeling accuracy (Acc.) in each of the evaluation cohorts*

| Artery | Paper I | | Paper II (Cohort 1) | | Paper II (Cohort 2) | | Paper III | |
|---|---|---|---|---|---|---|---|---|
| | No. Arteries | Acc. [%] | No. Arteries | Acc. [%] | No. Arteries | Acc. [%] | No. Arteries | Acc. [%] |
| ICA C2 | 134 | 100 | 334 | 99 | 20 | 100 | 73 | 97 |
| ICA C4 | - | - | - | - | - | - | 71 | 100 |
| BA | 67 | 97 | 166 | 98 | 10 | 100 | 38 | 100 |
| VA | 133 | 89 | 307 | 88 | 20 | 90 | 66 | 84 |
| PCA P1 | - | - | - | - | - | - | 66 | 65 |
| PCAP2 | 134 | 97 | 331 | 99 | 20 | 90 | 75 | 95 |
| PCoA | 60 | 70 | 80 | 91 | 5 | 75 | 25 | 71 |
| MCA | 134 | 100 | 334 | 100 | 20 | 100 | 76 | 88 |
| Distal MCA | - | - | 322 | 92 | 20 | 90 | - | - |
| ACA | 134 | 97 | 319 | 98 | 20 | 100 | 69 | 92 |
| Distal ACA | 67 | 96 | 167 | 100 | 20 | 90 | - | - |
| Total | | 93 | | 96 | | 93 | | 87 |

## Flow quantification

The agreement between manual and automatic measurements in Paper III was high, with no systematic difference in mean flow (0.61 ± 10.7 ml/min, p=0.21, Figure 5). When looking at individual arteries, the mean flow differences over all subjects were less than four percent for all arteries. Intraclass correlation was over 0.95 for all arteries, both for manual versus automatic and between the two raters.

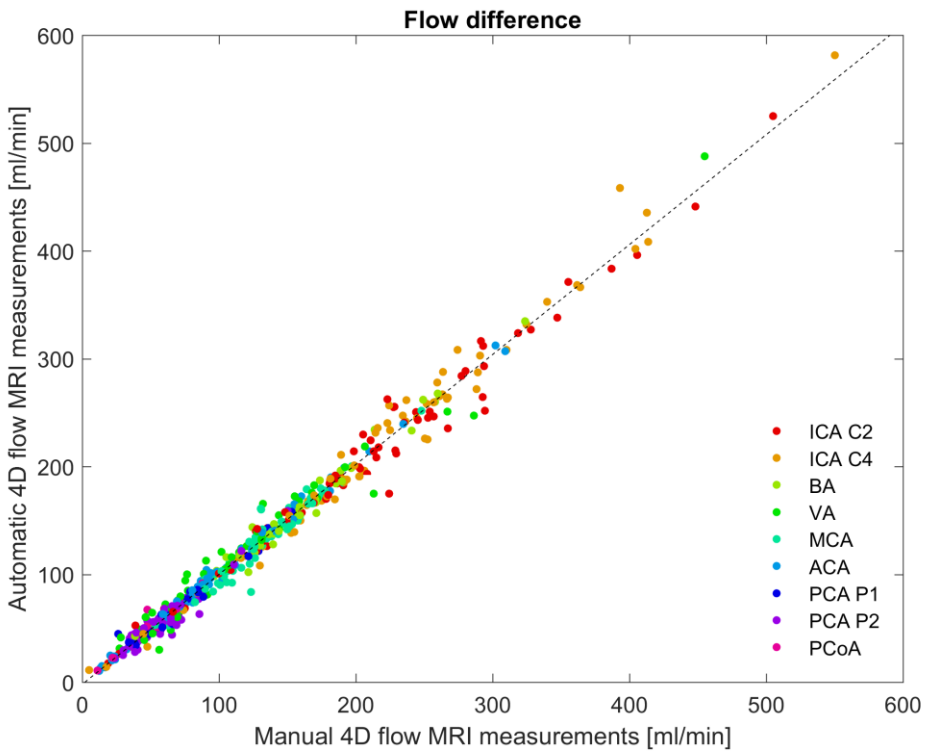


**Figure 5:** *Correlation between automatic and manual measurements (r=0.99). Linear regression (dashed line) revealed the relationship: Automatic flow = 1.02×Manual flow – 1.95*

In Paper IV, methods based on k-means clustering or local or global thresholding were validated against 2D PCMRI. All clustering methods showed a large underestimation in mean flow compared to 2D PCMRI (16-22 ml/min, Figure

6a), and a positive flow dependency, i.e. a larger underestimation of blood flow in larger arteries (slope = -0.09 to -0.19, r=0.37 to 0.62, p<0.001, Figure 6c).

In addition to the analyses presented in Paper IV, the FRQ from Paper III was compared to 2D PCMRI and evaluated in the same way, showing an overall ICC of 0.97 and a mean flow difference of -3.9 ± 17.5 ml/min (2D-4D) (Figure 6a, b and d). This flow difference was statistically significant (p<0.001), but still within an acceptable range considering the median value in the 2D PCMRI reference was 103 ml/min (interquartile range = 92.3 ml/min).

A large advantage of the thresholding methods compared to the clustering was that the threshold value could be fine-tuned to completely remove the systematic flow difference on group level. Optimal threshold levels were found by minimizing the mean flow difference compared to 2D PCMRI, and the resulting threshold levels were 10% for the global thresholding (-0.07 ± 17.3 ml/min) and 20% for the local thresholding (-0.04 ± 15.1), both with an ICC of 0.97. Regarding variability, local thresholding had a better concordance with 2D PCMRI (p=0.009, F-test). The local thresholding did also have a narrower range of flow differences for the different arteries (Table 1 in Paper IV) compared to global thresholding and FRQ. It was also the only method that did not have a significant flow dependency (r=-0.1, p=0.08, Figure 6c), suggesting that local thresholding is more robust to differences in vessel size. Figure 7 shows the excellent correlation (r = 0.97) between 2D PCMRI and 4D flow MRI, calculated with the 20% local threshold.

Finally, the impact of averaging flow values over multiple cut-planes was evaluated for all three methods, showing that no improvement in mean flow difference or standard deviation of the flow difference was found (Table 5).

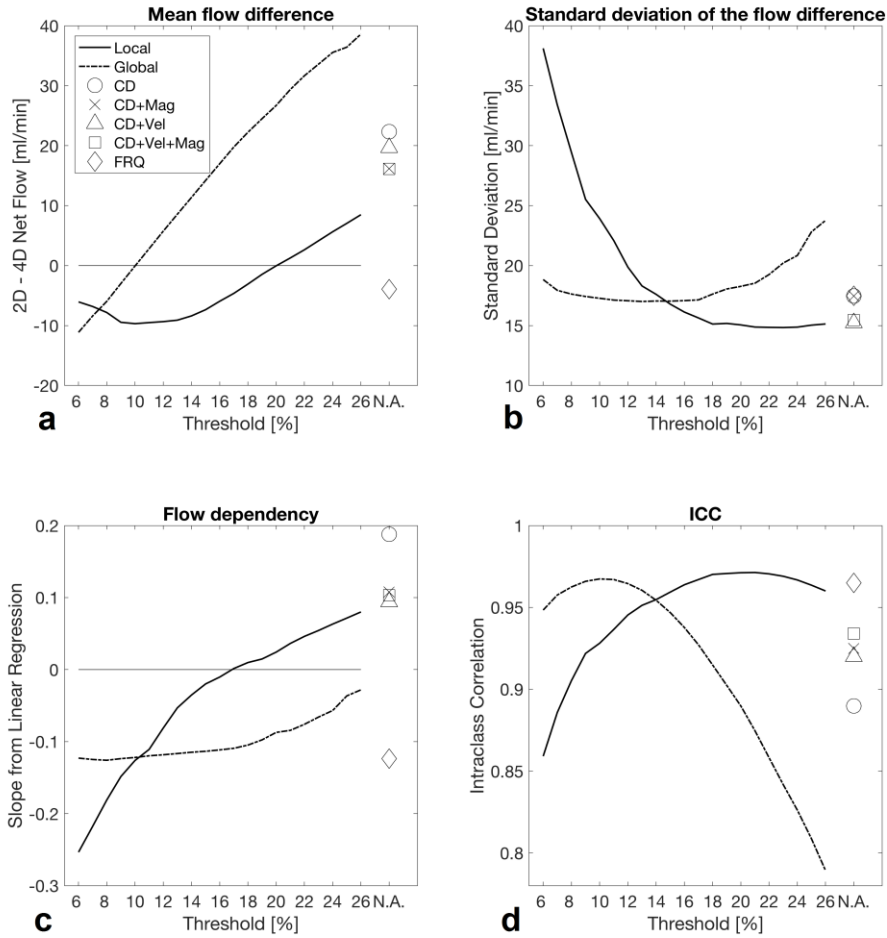


**Figure 6:** *Effects of different threshold levels with the local (solid line) and the global thresholding method (dash-dot line) when comparing 4D flow MRI to the 2D PCMRI measurements. Along with these methods, the clustering methods and the FRQ is included. a) Difference between 2D and 4D flow rate measurements [ml/min], b) Standard deviation of the flow difference [ml/min], c) Slope of a linear regression on flow difference vs. flow, d) Intraclass correlation (ICC(2,1)).*

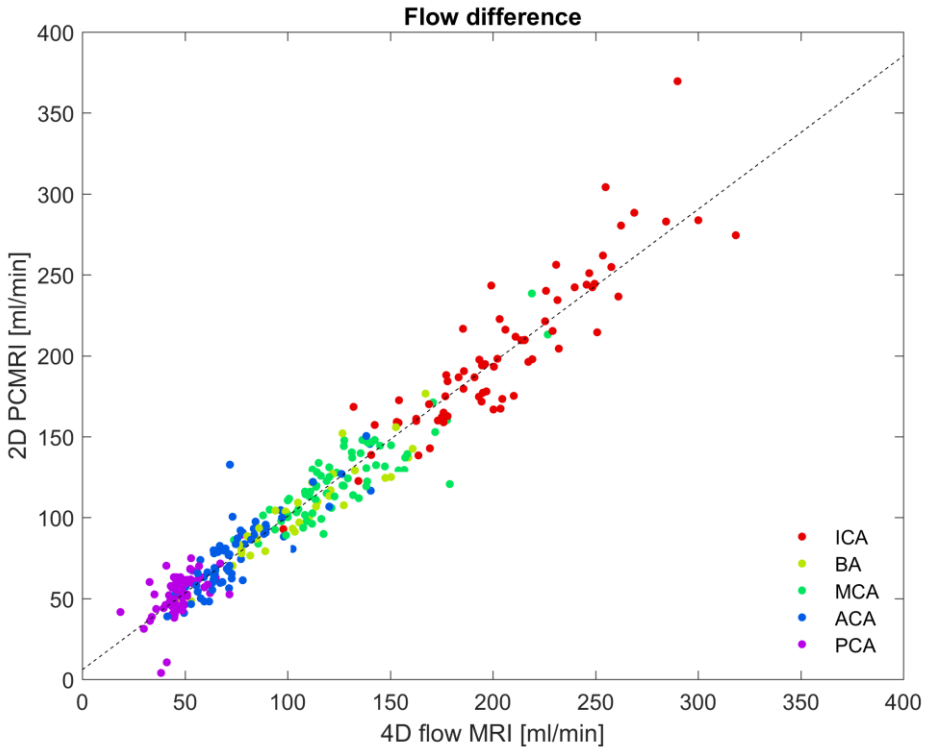


**Figure 7:** *Correlation between 2D PCMRI and 4D flow MRI (r=0.97) for 20% local threshold. Linear regression (dashed line) revealed the relationship: 4D flow= 0.95×2D flow + 5.94.*

**Table 5:** *Impact of segment length when averaging the flow rates of one, three or five cut-planes in three methods; local thresholding (20%), global thresholding (10%) and the FRQ. Flow rate difference [ml/min], standard deviation (SD) of the flow difference [ml/min] and ICC between 2D PCMRI and 4D flow MRI is presented for all arteries. No significant differences were found for any method*

| No. | Local threshold (20%) | | Global threshold (10%) | | FRQ | |
|---|---|---|---|---|---|---|
| Cut-planes | Flow diff ± SD | ICC | Flow diff ± SD | ICC | Flow diff ± SD | ICC |
| 1 | -0.04 ± 15.1 | 0.971 | -0.07 ± 17.3 | 0.967 | -3.9 ± 17.5 | 0.965 |
| 3 | 0.09 ± 15.2 | 0.971 | 0.37 ± 17.6 | 0.966 | -3.9 ± 17.3 | 0.966 |
| 5 | 0.23 ± 15.3 | 0.970 | 0.50 ± 17.7 | 0.966 | -3.9 ± 17.2 | 0.966 |

# Discussion

The aim of this thesis was to develop an automatic method for estimation of blood flow in cerebral arteries, measured with 4D flow MRI. The first goal was to construct a method for automatic labeling of cerebral arteries. We hypothesized that an atlas-based approach[14] would be suitable for this, and hence developed the AAIM (Paper I), including the arterial atlas UBA167 (Paper II). Paper I and II showed that the AAIM had a labeling accuracy of more than 90% when looking at all arteries together, and close to 100% for the largest cerebral arteries. The second goal focused on flow quantification, and included further developments of the AAIM to better control placement of the measurement in a pre-specified part of the artery (Paper III). When automatic flow quantification was compared to manual measurements, the average flow rate difference was less that one milliliter per minute. For further improvements, different approaches for arterial segmentation and flow quantification were compared to 2D PCMRI. Local thresholding based on intensity values from the CD, adapted for each measurement plane, performed better than both k-means clustering and a fixed threshold based on intensity values from the whole image (Paper IV).

In summary, this thesis presents a useful tool for automatic processing of 4D flow MRI data, making it possible to quantify flow in specific cerebral arteries with high accuracy. This new method is ready to be used for fast analysis of large data sets in a standardized way, and to evaluate how the 4D flow technique should be implemented in clinical practice.

## Developing the AAIM

When determining what constitutes an effective tool, several things need to be considered. First, the output values need to be reliable. They need to be as close to the true value as possible, and they need to be robust. By minimizing the manual input needed, stability between repeated measurements can be ensured. This also improves another aspect of effectiveness, i.e. time efficiency. A fully automated tool will both save time and remove inter- and intra-rater variability.

One large difference between arterial labeling and labeling of cerebral regions is that the shape of the vascular tree promotes skeleton extraction. This means that it is enough to label the voxels or even branches in the vascular skeleton; the full artery can be recreated from the labeled branch using vascular segmentation. Therefore, high accuracy labeling could be obtained based only on spatial probabilities, without the need for a priori assumptions about size, shape, or placement relative to other arteries, making the AAIM robust to anatomical and physiological variations.

Probabilistic atlases are widely used for labeling of brain tissue[14,15,110], and in this thesis, it is shown that the same approach was useful for arterial labeling. The UBA24 developed in Paper I was based on subjects with a specific vascular configuration, where all main arteries were present and had blood flow. This affected the generalizability of the atlas, since the material does not represent the population. By posing these restrictions on the material and therefore reducing the variation between subjects, fewer subjects were needed to construct a representative atlas, which is suitable for a proof of concept study. The high labeling accuracy in Paper I (Table 4), and the fact that only one of the PCoA that the AAIM failed to identify was of fetal type (Paper I), indicates that the UBA24 was still sufficient for arterial labeling even in subjects with morphological deviations. These findings prompted us to construct a more comprehensive atlas.

The largest difference between UBA167 and previous arterial atlases[66] is that it combined probabilistic and artery specific properties, meaning that different arteries are separated from each other, not just vessels from background or arteries from veins. Furthermore, when creating an atlas, it is important to use a suitable normalization method[111]. Paper II revealed that both agreement between subjects (AVR and maximum probability) and separation of arteries (dominating volume) was considerably improved by the DARTEL normalization, as compared to rigid-body transformation.

In addition to labeling, the UBA167 can potentially be used to remove vascular signal from functional MRI images or to provide a priori information for arterial

segmentation in other neuroimaging applications[112]. For this purpose, the ICA voxels that were present in all 167 subjects (Paper II) could be used as seed points for arterial automatic region growing segmentation methods[73].

In Paper I and II, the AAIM was designed to identify the whole artery; several labeled segments could therefore be combined to get the whole artery. This approach did not necessarily ensure true continuity of the labeled segments, and adjacent segments were not always joined in the correct order. When flow quantification was added, the need for well-defined segments increased, so the rules for which points were considered adjacent were tightened, and branches were no longer joined together, for the purpose of labeling single segments. The option for full-artery labeling is still available, and the AAIM has been improved to produce a truly continuous segment. This new full-artery labeling has shown positive results in non-published preliminary evaluations. To correctly measure blood flow in distal ACA and distal MCA, values from many arterial branches had to be summed. The AAIM does not allow identification of multiple branches, and these arterial regions were therefore omitted from Paper III.

## Interpretation of the arterial labeling

In Table 4, the labeling accuracy of the AAIM is presented. The AAIM was evaluated at three different time points during the development, for four different sets of subjects. No major changes were done to the labeling procedure in AAIM between Paper I and II, the main difference is the implementation of the UBA167. In Paper III, the goal of the labeling was shifted from identifying the whole artery to identifying a specific segment of the artery. This was done partly by discarding voxels that did not fall within specified atlas regions, and partly through stricter rules for what constituted a continuous segment of voxels.

Labeling accuracy was high for all groups, with values over 90% for most of the larger arteries. To calculate total cerebral blood flow, measurements from ICA and BA are needed; these arteries had accuracies close to 100% in all studies. Both ICA and BA are well separated from other arteries within the atlas, reducing the risk of mislabeling. The most cluttered region of the atlas is within the CoW,

particularly around P1 and PCoA, which are largely affected by their proximity to each other, and to P2, ICA and BA. These arteries did also present the lowest accuracy, followed by VA, which also shows large anatomical variation between subjects.

The changes made to the AAIM in Paper III did degrade the labeling results, especially for ACA and MCA. In ACA, several segments fell below the seven-voxel length-limit, and for MCA, the rules of what was considered a correct labeling was changed to only allow pre-bifurcation MCA (Table 3). In some subjects where the first MCA bifurcation occurred very early, the skeleton branch corresponding to this segment did not fulfill the seven-voxel length-limit even with perfect labeling. The purpose of this limit was to decrease the number of incorrectly labeled segments. By using a more inclusive length-limit, the sensitivity of the AAIM would increase, but to the cost of a decreased specificity. The level of seven voxels was selected based on assumptions made in Paper I and II, but a post hoc analysis comparing the accuracy for different length-limits suggested that this was a suitable value.

The placement of the VA atlas region in Paper III was problematic, since the only straight segment where the left and right VA was sufficiently separated from each other happened to coincide with the departure of the posterior inferior cerebral artery (Figure 3b), resulting in mislabeled segments. Similar errors were found in Paper I and II, but a subjective decision was made in each case to decide if the mislabeling was substantial or not. This decision was made with a generous approach; the praxis was to allow inclusion of the posterior inferior cerebral artery, as long as the target segment was also included.

The most striking difference between the four evaluated cohorts was the high PCoA accuracy for Paper II, Cohort 1, caused by the difference in the manual references used to determine which arteries does and does not exist. In this group, only arteries with enough blood flow to be visible in the binary image, and hence included in the atlas, were considered existing. This can be compared to Paper I, where existence of arteries was decided based on the magnitude image,

where practically no flow at all is needed for an artery to be visible. In Paper II, Cohort 2, the existence of arteries was determined based on CTA, and in Paper III the CD. In both these cases blood flow through the artery is needed for an artery to be visible, but there is no fixed level it must exceed, which is the case for the binary image. This does not have a big impact on the labeling accuracy for large arteries with substantial blood flow, but is very evident for small arteries such as PCoA, where flow rate is often low.

The supplementary analysis in Paper I showed that more than half of the incorrectly labeled segments were cases were the correct segments were lost in the initial thresholding of the tMIP, and the rest were almost evenly distributed between the box filtering and the labeling process. This analysis did not take in to account any additional errors that might be introduced if filtering was omitted or a different segmentation method was employed. In Paper III and IV, a new method for binarization of the angiographic image was implemented, this method improved the visibility of small arteries, and should hence increase the number of arteries that could be find in the labeling, but no formal comparison has been done.

## Flow quantification

Paper III showed an excellent agreement between automatically and manually placed measurements, supporting the use of the AAIM for flow assessment. The largest difference was found for PCA and VA, indicating that the positioning of these regions was not optimal, but even in those cases, the systematic flow difference was less than four percent of the mean flow in the artery. Intraclass correlations between automatic and manual measurements for ICA and VA was comparable to inter-rater values from 2D PCMRI[113].

When deciding what methods to include in Paper IV, one of the main criteria was that no manual input should be needed, which ruled out some of the more widely used methods[13,114]. The included methods were limited to clustering and thresholding approaches.

The FRQ used in Paper III is essentially a global thresholding method, with a threshold of 10%. The difference between the FRQ and the global thresholding method from Paper IV is that the FRQ calculates the flow rate directly in 3D space[16] instead of segmenting the vessel in an interpolated 2D plane (Paper IV). The FRQ performed at the same level as the 10% global thresholding method from Paper IV, in terms of standard deviation, flow dependency, and ICC (Figure 6, Table 5), but there was a minor systematic difference in flow compared to 2D PCMRI. This means that the precision of the flow quantification method was not improved by the interpolation and extraction of a 2D-plane, but the accuracy might be. In summary, the good agreement between FRQ and 2D PCMRI revealed that studies that use the FRQ produce reliable flow data comparable to the results global thresholding[16,115].

Local thresholding was the only method that did not generate a significant flow dependency i.e. correlation between flow difference and flow rate. This method did also have a lower standard deviation and a narrower range of flow differences than global thresholding. We found that a threshold value of 20% eliminated the mean difference between 2D PCMRI and 4D flow MRI, and this value was therefore recommended for future use.

When comparing results from a single cut-plane to values averaged over several cut-planes, no difference was found for any of the three evaluated methods (Table 5). This indicates that the difference between 2D PCMRI and 4D flow MRI was not caused by insufficient SNR of the 4D flow MRI, but rather physiological differences in flow between the two time-points when the measurements were performed. It is important to note that these values were based on mean blood flow over the cardiac cycle. For time-resolved data, SNR is lower, since each image is based on less data, and therefore averaging values over several cut-planes might still be advantageous.

All 4D flow MRI data used in this thesis was collected with a Venc of 110 cm/s. For the 2D PCMRI collection, Venc values between 60 and 100 cm/s were used. In two arteries (one BA and one ACA) aliasing was noted at the time of

measurement, and the measurement was repeated with a higher Venc. In some cases, aliasing was found in the 2D PCMRI during post-processing and was then corrected for. A higher Venc value could have eliminated aliasing all together, but to the cost of lower velocity-to-noise ratio (VNR), and an even lower labeling accuracy for PCoA and possibly PCA.

When analyzing the 2D PCMRI data in Paper IV, an oversized ROI was used to ensure that all flow values were included; furthermore, the ROI was kept constant over all time frames and therefore adjusted in size to include movement of the artery over the cardiac cycle. This movement is limited for cerebral arteries, and motion tracking was not considered necessary. Oversized ROIs are preferable when analyzing 2D PCMRI[96], and optimizing the 4D flow MRI segmentation to these 2D values did also result in oversized ROIs in the 4D flow MRI data. This can be seen by the 10% limit identified as optimal for the global thresholding, compared to the 18% threshold that was used for vascular skeleton extraction, and optimized to conservatively separate vessels from each other, and from background tissue[16].

## Advantage of 4D flow MRI

The main advantage of 4D flow MRI compared to 2D PCMRI is that data is sampled for the entire brain volume simultaneously, and the arteries of interest can be selected during post processing. With 2D PCMRI, a double-oblique measurement plane is placed for each artery, requiring anatomical knowledge and experience during scanning. Since each artery is measured separately with 2D PCMRI, settings, particularly the Venc, can be adjusted for each artery to improve VNR. For 4D flow MRI, the Venc will be the same for all arteries, resulting in a low VNR for small arteries. However, if many arteries of different sizes are to be investigated, 4D flow data can be collected with both high and low Venc, while still saving time compared to 2D PCMRI.

Both 4D flow MRI and 2D PCMRI produces time-resolved data, even though this property was not utilized in this work. This does not mean that the data is collected in real time, but that cardiac gating is used to arrange the data based on

where in the cardiac cycle it was sampled, and from that reconstruct images that describe the flow over an average cardiac cycle.

## Importance of physiological factors

In Paper III, manual and automatic measurements were done on the same data, using the same automatic method for defining the ROI; differences between measurements are therefore only based on the placement of the measurement seed points. This was not the case for Paper IV where data collection of 4D flow MRI was compared to 2D PCMRI, which was not collected simultaneously, and physiological parameters such as heart rate and blood pressure was an extra source of variability. An automated approach was used to match the locations of 4D flow MRI measurements to the ones specified by the 2D PCMRI analysis[51]. The offset found between these two data sets corresponded to a backwards tilt of the head, and was therefore larger for ACA and MCA, but since they have a lateral direction, and the shift was mainly in the anterior-posterior direction, the projection of the location on the arteries was mainly unaffected.

The ICC between 2D PCMRI and the suggested method of Paper IV was good (lower bound of the 95% confidence interval over 0.5) for all arteries except PCA, and excellent on the group level (ICC=0.97). This mismatch for the PCA is suspected to be partly due to physiological variation caused by changes in activity in the visual cortex of the occipital lobe, for example if the subjects eyes are open or closed[116]. The variation of blood flow rates in cerebral arteries is large[117], affecting the reproducibility of 2D PCMRI[118,119]. A previous study showed that repeated 2D PCMRI measurements in the ICA gave a within-subject variation of 20 ml/min[120]. The variation of the difference between 2D and 4D that we found was 22.5 ml/min for the right ICA and 19.4 ml/min in the left ICA, indicating that the variation we observed is dominated by true physiological variation.

PCA has a diameter of about 2 mm[121], which corresponds to three voxels in the 4D data and six voxels in the 2D data, this is approaching the limit for how small vessels can be reliably measured. For 2D PCMRI, a systematic error of 10% can be expected for vessels with a diameter of four voxels and 5% for five voxels[96,120].

Partial volume effect in 2D PCMRI is dependent on inflow effects, and can therefore not be directly translated to 4D flow MRI, since the proximal blood is also pre-exited in this case. This decreases the magnitude difference between blood and surrounding tissue in intracranial 4D flow MRI data with whole brain coverage, likely making the 4D flow partial volume overestimation less severe.

## Generalizability

Evaluations of the AAIM were done on gradually more severe vascular diseases, starting with a population-based material (Paper I and II), moving on to TIA and small vessel disease (Paper II), and further to carotid artery stenosis (Paper III). Both labeling accuracy and flow agreement was high for all investigated cohorts. The differences between groups seen in Table 4 have already been explained based on method or evaluation design (see *Interpretation of arterial labeling*). The robustness against deviating flow rates was supported by the high labeling accuracy in ICA for subjects with atherosclerosis, the artery where these deviations were the largest.

The difference in flow distribution between subjects with and without atherosclerosis can be seen by comparing the correlation plots in Figure 5 and 7, where the range of flow values for a specific artery is much smaller in the healthy subjects (Figure 7, Paper IV) than the subject with atherosclerosis (Figure 5, Paper III). This larger range of values did contribute to the high correlation at artery level, but did also show that the automatic labeling was insensitive to those variations and produced a high accuracy even for pathological flow levels.

The UBA167 was developed from a sample with a quite narrow age span, and the AAIM has only been evaluated for subjects in that age span or older, but we hypothesize that it would work even better in a younger sample, with a healthier cerebral vascular tree.

## Future work

The current output from the AAIM is a 3D image showing the labeled segments (Figure 3 b), and a list of flow values corresponding to the labeled segments. For

the AAIM to be clinically useful, values must be presented in a way that is easier to understand, Figure 8 shows an example of such an output image.

Even though the accuracy of the labeling was high, visual inspection of the labeling is needed to ensure that the presented values correspond to the correct segments. In connection to this visual inspection, it should also be possible to edit the position or make additional measurements in cases where the AAIM failed to identify an artery. This graphical editing tool is still under development, with several of the underlying functions ready to go.

The labeling errors can be divided into *not identified segments* and *mislabeled segments*. The first type of errors is more common and can easily be detected, since the AAIM indicates that the artery was not found. The second type is easier to miss, since a flow value is still presented, which is why an easily interpretable image for visual inspection is needed. By including morphological information in the labeling, some of the more common errors, for example in the PCA – PCoA bifurcation, could be automatically identified, giving the user an error message when segments are placed in an incorrect order.

4D flow MRI is not applicable in the acute setting, due to its long processing time, but it can still be useful for planning of treatment, such as stenting of stenotic brain arteries or carotids surgery[122,123]. The total computational run-time of the AAIM for one subject, as it is presented in Paper III, was just over an hour. About forty minutes of that time was the reconstruction of the data, which is needed for manual measurements as well. This processing time could be reduced by increasing computer power or with more effective programming. Since the AAIM runs automatically, this time can be devoted to other tasks, or even to run a larger batch of subjects overnight.

Even though we have only presented blood flow rates in ml/min, 4D flow MRI presents an appealing opportunity for analysis of advanced flow patterns[52,124]. In addition to mean blood flow rate, values such as maximum velocity and cross-sectional area can be calculated with the proposed methods. With time-resolved data, pulsatility and flow patterns over the cardiac cycle can be investigated;

analysis of time-resolved 4D flow MRI with the AAIM is thus a natural next step in the development process.

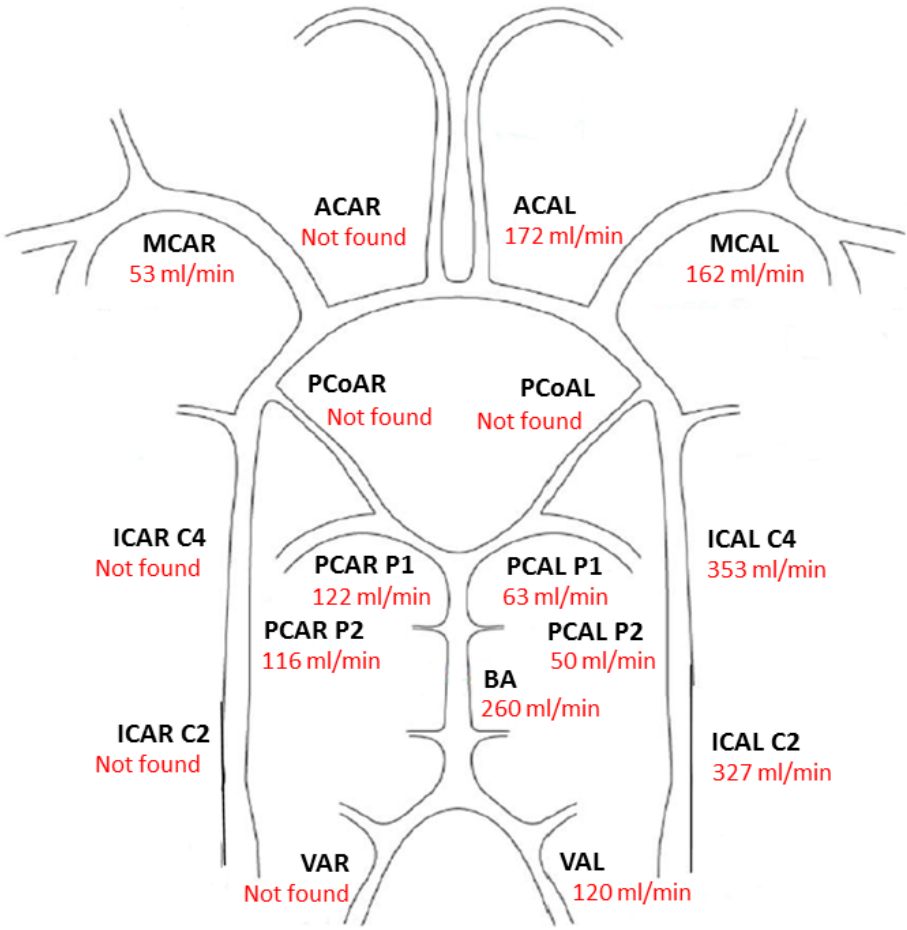


**Figure 8:** *Example of clinical output image in a subject with a carotid stenosis, blood flow rate is presented for each identified arterial segment*

# Conclusions

In this thesis, we present an automatic atlas-based arterial identification method (AAIM), a stereotactic probabilistic atlas based on 167 subjects (UBA167), and a method for accurate quantification of arterial blood flow rate, based on local thresholding.

The AAIM had a high labeling accuracy, in combination with both the preliminary UBA24 and the more extensive UBA167, suggesting that atlas-based labeling is well suited for automatic identification of cerebral arteries. When further developing the AAIM to include flow rate quantification in 4D flow MRI, the method showed an excellent agreement with manually placed measurements, revealing that the method was stable also for labeling of shorter arterial segments, and that it produces reliable flow rate estimations.

In addition to the AAIM and corresponding atlases, we have developed and described a method for intracranial 4D flow MRI vessel segmentation and flow quantification without systematic difference in mean flow, or dependency on flow rate compared to 2D PCMRI.

Together, these methods form a new instrument for processing intracranial 4D flow MRI, which is needed for implementation of 4D flow MRI in clinical practice. This instrument makes it possible to analyze large amounts of data in a short time, with results at the same level or better than manual processing, presenting flow values in multiple cerebral arteries in an accessible way.

# Acknowledgements

I would like to thank all my friends, coworkers and coauthors, who have helped me and supported me through this time. First of all, thanks to my supervisors Anders Eklund, Jan Malm and Anders Wåhlin for all of your support, I've realized that far from everybody have been so lucky.

Anders E, I could not have wished for a more supporting, helpful, encouraging and inspiring main supervisor. A PhD education is filled with ups and downs, and you have always made me feel like my work is worthwhile and that I actually do know some stuff.

Jan, thanks for connecting my research to the real word by asking all the hard questions and forcing me to express myself as clearly as possible. Being part of an interdisciplinary research group is something I have greatly appreciated, and you have always taken time out of your busy schedule to help me improve my work.

Anders W, thanks for all interesting, helpful and rewarding discussions and explanations about everything from MRI techniques to presentation of data. There is no way I would have understood all this stuff without you. Thanks for all the technical support, for face-timing my computer when the reconstruction process fails, and for all the MATLAB help when I was a newbie.

Thanks to Khalid Ambarki for being practically a fourth supervisor during my first years, devoting so much time and always having a paper in mind for every question.

Laleh Zarrinkoob, thanks for being my on-and-off-again roommate and all the help and interesting discussions. Out of all these "busy schedules", you probably have the busiest one, so every second spent on my research instead of your own is greatly appreciated.

Thanks to Madelene Holmgren for sharing the main responsibility of Paper IV with me, I would not have had time to finish this thesis without it. It was a lot of hard work and I really hope that your future research studies will run smoother, but I'm really happy with where we ended up.

Thanks to my other co-PhD-students and post-docs, particularly Sara Qvarlander and Petter Holmlund, for all support through this whole process. It's so important to have someone to talk to and compare experiences with.

Thanks to all my coworkers at MT-FoU, to the research group, the people at the neurological department and the research camera, particularly Kristin Nyman and Rebeca de Peredo Axelsson, there is so much work that goes unnoted but it really takes a village to do research.

Thanks to Oliver Wieben and the MRI flow group at UW Madison for welcoming me last spring, I learned so much in those two months, not only about PCVIPR but about being a researcher in general.

Thanks to Maria Wing and Margareta Marklund at the Radiation Science department, as well as the people at the Deans office at the Medical faculty, for answering all of my stupid questions and helping me with all the administrative stuff.

Thanks to UFBI for really bringing my interest for cognitive neuroscience to life, and to Lars Nyberg and the COBRA-team for access to the data, without it there would be no atlas.

Thanks to all of my friends and family of course, both in Umeå and everywhere else. I'm so lucky to feel at home in so many places.

This thesis was financed by the Swedish Research Council [grant number 2015–05616], the Swedish Heart and Lung Foundation [grant numbers 20110383, 20140592] and the Swedish Brain Foundation. A grant from the Swedish Research Council [grant number 421-2012-648] to Lars Nyberg supported the COBRA data collection.

The atlases can be downloaded at http://www.nitrc. org/projects/brainarteries

# References


1. Rothwell PM, Coull AJ, Silver LE, et al. Population-based study of event-rate, incidence, case fatality, and mortality for all acute vascular events in all arterial territories (Oxford Vascular Study). *Lancet*. 2005;366:1773-1783. doi:10.1016/S0140-6736(05)67702-1.

2. Berman SE, Rivera-Rivera LA, Clark LR, et al. Intracranial arterial four-dimensional flow is associated with metrics of brain health and Alzheimer's disease. *Alzheimer's Dement Diagnosis, Assess Dis Monit*. 2015;1(4):420-428. doi:10.1016/j.dadm.2015.09.005.

3. Sabayan B, Jansen S, Oleksik AM, et al. Cerebrovascular hemodynamics in Alzheimer's disease and vascular dementia: a meta-analysis of transcranial Doppler studies. *Ageing Res Rev*. 2012;11(2):271-277. doi:10.1016/j.arr.2011.12.009.

4. Benedictus MR, Leeuwis AE, Binnewijzend MAA, et al. Lower cerebral blood flow is associated with faster cognitive decline in Alzheimer's disease. *Eur Radiol*. 2016. doi:10.1007/s00330-016-4450-z.

5. Hays CC, Zlatar ZZ, Wierenga CE. The Utility of Cerebral Blood Flow as a Biomarker of Preclinical Alzheimer's Disease. *Cell Mol Neurobiol*. 2016. doi:10.1007/s10571-015-0261-z.

6. Rubin G, Firlik AD, Levy EI, Pindzola RR, Yonas H. Relationship between cerebral blood flow and clinical outcome in acute stroke. *Cerebrovasc Dis*. 2000;10(4):298-306. http://www.ncbi.nlm.nih.gov/pubmed/10878436.

7. Amin-Hanjani S, Pandey DK, Rose-Finnell L, et al. Effect of Hemodynamics on Stroke Risk in Symptomatic Atherosclerotic Vertebrobasilar Occlusive Disease. *JAMA Neurol*. 2016;73(2):178-185. doi:10.1001/jamaneurol.2015.3772.

8. Liebeskind DS. Collateral circulation. *Stroke*. 2003;34(9):2279-2284. doi:10.1161/01.STR.0000086465.41263.06.

9. Krabbe-Hartkamp MJ, van der Grond J, de Leeuw F-E, et al. Circle of Willis: Morphologic Variation on Three-dimensional Time-of-Flight MR Angiograms. *Radiology*. 1998;207(1):103-111.

10. Gu T, Korosec FR, Block WF, et al. PC VIPR: a high-speed 3D phase-contrast method for flow quantification and high-resolution angiography. *Am J Neuroradiol*. 2005;26(4):743-749. http://www.ncbi.nlm.nih.gov/pubmed/15814915.

11. Markl M, Frydrychowicz A, Kozerke S, Hope M, Wieben O. 4D flow MRI. *J Magn Reson Imaging*. 2012;36(5):1015-1036. doi:10.1002/jmri.23632.

12. Tariq U, Hsiao A, Alley M, Zhang T, Lustig M, Vasanawala SS. Venous and arterial flow quantification are equally accurate and precise with parallel imaging compressed sensing 4D phase contrast MRI. *J Magn Reson Imaging*. 2013;37(6):1419-1426. doi:10.1002/jmri.23936.

13. Stalder AF, Russe MF, Frydrychowicz A, Bock J, Hennig J, Markl M. Quantitative 2D and 3D phase contrast MRI: Optimized analysis of blood flow and vessel wall parameters. *Magn Reson Med*. 2008;60(5):1218-1231. doi:10.1002/mrm.21778.

14. Ashburner J, Friston KJ. Unified segmentation. *Neuroimage*. 2005;26(3):839-851. doi:10.1016/j.neuroimage.2005.02.018.

15. Diedrichsen J, Balsters JH, Flavell J, Cussans E, Ramnani N. A probabilistic MR atlas of the human cerebellum. *Neuroimage*. 2009;46(1):39-46. doi:10.1016/j.neuroimage.2009.01.045.

16. Wåhlin A, Ambarki K, Birgander R, et al. Measuring Pulsatile Flow in Cerebral Arteries Using 4D Phase-Contrast MR Imaging. *Am J Neuroradiol*. 2013;34:1740-1745. doi:10.3174/ajnr.A3442.

17. Schrauben E, Wåhlin A, Ambarki K, et al. Fast 4D flow MRI intracranial segmentation and quantification in tortuous arteries. *J Magn Reson Imaging*. 2015;42(5):1458-1464. doi:10.1002/jmri.24900.

18. Dyverfeldt P, Bissell M, Barker AJ, et al. 4D flow cardiovascular magnetic resonance consensus statement. *J Cardiovasc Magn Reson*. 2015;17(1):72. doi:10.1186/s12968-015-0174-5.

19. Winship IR. Cerebral Collaterals and Collateral Therapeutics for Acute Ischemic Stroke. *Microcirculation*. 2015;22(3):157-236. doi:10.1111/micc.12177.

20. Iqbal S. A comprehensive study of the anatomical variations of the circle of willis in adult human brains. *J Clin Diagnostic Res*. 2013;7(11):2423-2427. doi:10.7860/JCDR/2013/6580.3563.

21. Tanaka H, Fujita N, Enoki T, et al. Relationship between variations in the circle of Willis and flow rates in internal carotid and basilar arteries determined by means of magnetic resonance imaging with semiautomated lumen segmentation: reference data from 125 healthy volunteers. *Am J Neuroradiol*. 2006;27(8):1770-1775. http://www.ncbi.nlm.nih.gov/pubmed/16971634.

22. Qiu C, Zhang Y, Xue C, Jiang S, Zhang W. MRA Study on Variation of the Circle of Willis in Healthy Chinese Male Adults. *Biomed Res Int*. 2015;2015.

23. Osborn AG. *Diagnostic Cerebral Angiography*. 2nd ed. Philadelphia: Lippincott Williams & Wilkins; 1999.

24. Sano A, Hirano T, Watanabe K, et al. Preoperative evaluation of the vertebral arteries and posterior portion of the circle of Willis for cervical spine surgery using 3-dimensional computed tomography angiography. *Spine (Phila Pa 1976)*. 2013;38(15):E960-7. doi:10.1097/BRS.0b013e318296e542.

25. Brynolfsson C, ed. *Neurologi*. 4th ed. Falköping; 2006.

26. Runge VM. *Imaging of Cerbrovascular Diseases : A Practical Guide*. 1st ed. (Lamsback W, ed.). New York: Thieme; 2016.

27. Saczynski JS, Sigurdsson S, Jonsdottir MK, et al. Cerebral Infarcts and Cognitive Performance: Importance of Location and Number of Infarcts. *Stroke*. 2009;40(3):677-682. doi:10.1161/STROKEAHA.108.530212.

28. Warlow C, Gijn J van, Dennis M, et al. *Stroke: Practical Management*. 3rd ed. Blackwell Publishing; 2008.

29. Giles MF, Rothwell PM. Risk of stroke early after transient ischaemic attack : a systematic review and meta-analysis. *Lancet Neurol*. 2007;6:1063-1072. doi:10.1016/S1474-4422(07)70274-0.

30. Rothwell PM, Buchan A, Johnston SC. Recent advances in management of transient ischaemic attacks and minor ischaemic strokes. *Lancet Neurol*. 2006;5(4):323-331.

31. Schellinger PD, Richter G, Köhrmann M, Dörfler A. Update in Diagnostic Procedures : Noninvasive Angiography (Magnetic Resonance and Computed Tomography) in the Diagnosis of Ischemic Cerebrovascular Disease. *Cerebrovasc Dis*. 2007;24(suppl 1):16-23. doi:10.1159/000107375.

32. Agarwal R, Brunelli SM, Williams K, Mitchell MD, Feldman HI, Umscheid CA. Gadolinium-based contrast agents and nephrogenic systemic fibrosis : a systematic review and meta-analysis. *Nephrol Dial Transpl*. 2009;(24):856-863. doi:10.1093/ndt/gfn593.

33. Kortman HGJ, Smit EJ, Oei MTH, Manniesing R, Prokop M, Meijer FJA. 4D-CTA in neurovascular disease: A review. *Am J Neuroradiol*. 2015;36(6):1026-1033. doi:10.3174/ajnr.A4162.

34. Xu J, Shi D, Chen C, et al. Noncontrast-Enhanced Four-Dimensional MR Angiography for the Evaluation of Cerebral Arteriovenous Malformation : A Preliminary Trial. *J Immunol Methods*. 2011;34:1199-1205. doi:10.1002/jmri.22699.

35. Rinck PA. *Magnetis Resonance in Medicine*. 4th ed. (Peter A Rinck, ed.). Minusio, Switzerland: EMRF foundation; 2001.

36. Bernstein MA, King KE, Zhou XJ, Fong W. *Handbook of MRI Pulse Sequences*. Vol 32. Burlington, Vermont: Academic Press; 2005.

37. Stanisz GJ, Odrobina EE, Pun J, et al. T1, T2 Relaxation and Magnetization Transfer in Tissue at 3T. *Magn Reson Med*. 2005;54:507-512. doi:10.1002/mrm.20605.

38. Lu H, Clingman C, Golay X, Zijl PCM Van. Determining the Longitudinal Relaxation Time (T1) of Blood at 3.0 Tesla. *Magn Reson Med*. 2004;52:679-682. doi:10.1002/mrm.20178.

39. Greenman RL, Shirosky JE, Mulkern R V, Rofsky NM. Double Inversion Black-Blood Fast Spin-Echo Imaging of the Human Heart : A Comparison. *J Magn Reson Imaging*. 2003;17:648-655. doi:10.1002/jmri.10316.

40. Bojorquez JZ, Bricq S, Acquitter C, Brunotte F, Walker PM, Lalande A. What are normal relaxation times of tissues at 3 T? *Magn Reson Imaging*. 2017;35:69-80. doi:10.1016/j.mri.2016.08.021.

41. Markl M, Leupold J. Gradient Echo Imaging. *J Magn Reson Imaging*. 2012;1289:1274-1289. doi:10.1002/jmri.23638.

42. Deshmane A, Gulani V, Griswold MA, Seiberlich N. Parallel MR Imaging. *J Magn Reson Imaging*. 2012;36(1):55-72. doi:10.1002/jmri.23639.

43. Van Ooij P, Zwanenburg JJM, Visser F, et al. Quantification and visualization of flow in the Circle of Willis: Time-resolved three-dimensional phase contrast MRI at 7 T compared with 3 T. *Magn Reson Med*. 2013;69(3):868-876. doi:10.1002/mrm.24317.

44. Bazzocchi M, Quaia E, Zuiani C, Moroldo M. Transcranial Doppler : state of the art. *Eur J Radiol*. 1998;27:141-148.

45. Spilt A, Box FMA, Geest RJ Van Der, et al. Reproducibility of Total Cerebral Blood Flow Measurements Using Phase Contrast Magnetic Resonance Imaging. *J Magn Reson Imaging*. 2002;16:1-5. doi:10.1002/jmri.10133.

46. Best LMJ, Webb AC, Gurusamy KS, Cheng SF, Richards T. Transcranial Doppler Ultrasound Detection of Microemboli as a Predictor of Cerebral Events in Patients with Symptomatic and Asymptomatic Carotid Disease : A Systematic Review and Meta-Analysis. *Eur J Vasc Endovasc Surg*. 2016;52(5):565-580. doi:10.1016/j.ejvs.2016.05.019.

47. Nett EJ, Johnson KM, Frydrychowicz A, et al. Four-dimensional phase contrast MRI with accelerated dual velocity encoding. *J Magn Reson Imaging*. 2012;35(6):1462-1471. doi:10.1002/jmri.23588.

48. Meckel S, Leitner L, Bonati LH, et al. Intracranial artery velocity measurement using 4D PC MRI at 3 T: comparison with transcranial ultrasound techniques and 2D PC MRI. *Neuroradiology*. 2013;55(4):389-398. doi:10.1007/s00234-012-1103-z.

49. Stankovic Z, Allen BD, Garcia J, Jarvis KB, Markl M. 4D flow imaging with MRI. *Cardiovasc Diagn Ther*. 2014;4(2):173-192. doi:10.3978/j.issn.2223-3652.2014.01.02.

50. Sigfridsson A, Petersson S, Carlhäll CJ, Ebbers T. Four-dimensional flow MRI using spiral acquisition. *Magn Reson Med*. 2012;68(4):1065-1073. doi:10.1002/mrm.23297.

51. Carlsson M, Töger J, Kanski M, et al. Quantification and visualization of cardiovascular 4D velocity mapping accelerated with parallel imaging or k-t BLAST: head to head comparison and validation at 1.5 T and 3 T. *J Cardiovasc Magn Reson*. 2011;13(1):55. doi:10.1186/1532-429X-13-55.

52. Frydrychowicz A, François CJ, Turski PA. Four-dimensional phase contrast magnetic resonance angiography: potential clinical applications. *Eur J Radiol*. 2011;80(1):24-35. doi:10.1016/j.ejrad.2011.01.094.

53. Schnell S, Wu C, Ansari SA. Four-dimensional MRI flow examinations in cerebral and extracerebral vessels – ready for clinical routine? *Curr Opin Neurol*. 2016:1-10. doi:10.1097/WCO.0000000000000341.

54. François CJ, Srinivasan S, Schiebler ML, et al. 4D cardiovascular magnetic resonance velocity mapping of alterations of right heart flow patterns and main pulmonary artery hemodynamics in tetralogy of Fallot. *J Cardiovasc Magn Reson*. 2012;14(1):16. doi:10.1186/1532-429X-14-16.

55. Frydrychowicz A, Landgraf BR, Niespodzany E, et al. Four-dimensional velocity mapping of the hepatic and splanchnic vasculature with radial sampling at 3 tesla: a feasibility study in portal hypertension. *J Magn Reson Imaging*. 2011;34(3):577-584. doi:10.1002/jmri.22712.

56. Nilsson A, Bloch KM, Töger J, Heiberg E, Ståhlberg F. Accuracy of four-dimensional phase-contrast velocity mapping for blood flow visualizations: a phantom study. *Acta radiol*. 2013;54:663-671. doi:10.1177/0284185113478005.

57. Yamashita S, Isoda H, Hirano M, et al. Visualization of hemodynamics in intracranial arteries using time-resolved three-dimensional phase-contrast MRI. *J Magn Reson Imaging*. 2007;25:473-478. doi:10.1002/jmri.20828.

58. Wetzel S, Meckel S, Frydrychowicz A, Bonati L, Radue E. In Vivo Assessment and Visualization of Intracranial Arterial Hemodynamics with Flow- Sensitized 4D MR Imaging at 3T. *Am J Neuroradiol*. 2007;28:433-438.

59. Meckel S, Stalder AF, Santini F, Radü E, Wetzel SG. In vivo visualization and analysis of 3-D hemodynamics in cerebral aneurysms with flow-sensitized 4-D MR imaging at 3 T. *Neuroradiology*. 2008;50:473-484. doi:10.1007/s00234-008-0367-9.

60. Walcott BP, Reinshagen C, Stapleton CJ, et al. Predictive modeling and in vivo assessment of cerebral blood flow in the management of complex cerebral aneurysms. *J Cereb Blood Flow Metab*. 2016. doi:10.1177/0271678X16641125.

61. Rivera-Rivera LA, Turski P, Johnson KM, et al. 4D flow MRI for intracranial hemodynamics assessment in Alzheimer's disease. *J Cereb Blood Flow Metab*. 2016;36(10):1718-1730. doi:10.1177/0271678X15617171.

62. Evans AC, Janke AL, Collins DL, Baillet S. Brain templates and atlases. *Neuroimage*. 2012;62(2):911-922. doi:10.1016/j.neuroimage.2012.01.024.

63. Ashburner J. A fast diffeomorphic image registration algorithm. *Neuroimage*. 2007;38(1):95-113. doi:10.1016/j.neuroimage.2007.07.007.

64. Nowinski WL, Gupta V, Qian G, Ambrosius W, Kazmierski R. Population-Based Stroke Atlas for Outcome Prediction: Method and Preliminary Results for Ischemic Stroke from CT. *PLoS One*. 2014;9(8):1-11. doi:10.1371/journal.pone.0102048.

65. Nowinski WL. 3D Atlas of the Brain, Head and Neck in 2953 pieces. *Neuroinformatics*. 2017. doi:10.1007/s12021-017-9339-8.

66. Nowinski WL. Human brain atlasing: past, present and future. *Neuroradiol J*. 2017;0(0):1-16. doi:10.1177/1971400917739274.

67. Nowinski WL, Chua BC, Marchenko Y, Puspitsari F, Volkau I, Knopp M V. Three-dimensional reference and stereotactic atlas of human cerebrovasculature from 7 Tesla. *Neuroimage*. 2011;55(3):986-998. doi:10.1016/j.neuroimage.2010.12.079.

68. Mut F, Wright S, Ascoli GA, Cebral JR. Morphometric, geographic, and territorial characterization of brain arterial trees. *Int J Numer Method Biomed Eng*. 2014;30:755-766. doi:10.1002/cnm.

69. Forkert ND, Fiehler J, Suniaga S, Wersching H, Knecht S, Kemmling A. A statistical cerebroarterial atlas derived from 700 MRA datasets. *Methods Inf Med*. 2013;52(6):467-474. doi:10.3414/ME13-02-0001.

70. Wright SN, Kochunov P, Mut F, et al. Digital reconstruction and morphometric analysis of human brain arterial vasculature from magnetic resonance angiography. *Neuroimage*. 2013;82:170-181. doi:10.1016/j.neuroimage.2013.05.089.

71. Cabezas M, Oliver A, Llado X, Freixenet J, Bach Cuadra M. A review of atlas-based segmentation for magnetic resonance brain images. *Comput Methods Programs Biomed*. 2011;104(3):e158-e177. doi:10.1016/j.cmpb.2011.07.015.

72. Taso M, Le Troter A, Sdika M, et al. Construction of an in vivo human spinal cord atlas based on high-resolution MR images at cervical and thoracic levels: Preliminary results. *Magn Reson Mater Phy*. 2014;27(3):257-267. doi:10.1007/s10334-013-0403-6.

73. Passat N, Ronse C, Baruthio J, Armspach J-P, Maillot C, Jahn C. Region-growing segmentation of brain vessels: an atlas-based automatic approach. *J Magn Reson Imaging*. 2005;21(6):715-725. doi:10.1002/jmri.20307.

74. Bustamante M, Petersson S, Eriksson J, et al. Atlas-based analysis of 4D flow CMR: Automated vessel segmentation and flow quantification. *J Cardiovasc Magn Reson*. 2015;17(1):87. doi:10.1186/s12968-015-0190-5.

75. Bogunovic H, Pozo JM, Cárdenes R, San Román L, Frangi AF. Anatomical labeling of the Circle of Willis using maximum a posteriori probability estimation. *IEEE Trans Med Imaging*. 2013;32(9):1587-1599. doi:10.1109/TMI.2013.2259595.

76. Bilgel M, Roy S, Carass A, Nyquist PA, Prince JL. Automated Anatomical Labeling of the Cerebral Arteries Using Belief Propagation. *Proc SPIE Int Soc Opt Eng*. 2013;866918:1-6. doi:10.1117/12.2006460.

77. Ghanavati S, Lerch JP, Sled JG. Automatic anatomical labeling of the complete cerebral vasculature in mouse models. *Neuroimage*. 2014;95:117-128. doi:10.1016/j.neuroimage.2014.03.044.

78. Suri JS, Liu K, Reden L, Laxminarayan S. A review on MR vascular image processing algorithms: acquisition and prefiltering: part I. *IEEE Trans Inf Technol Biomed*. 2002;6(4):324-337. http://www.ncbi.nlm.nih.gov/pubmed/15224847.

79. Suri JS, Liu K, Reden L, Laxminarayan S. A review on MR vascular image processing: skeleton versus nonskeleton approaches: part II. *IEEE Trans Inf Technol Biomed*. 2002;6(4):338-350. http://www.ncbi.nlm.nih.gov/pubmed/15224848.

80. Flasque N, Desvignes M, Constans J-M, Revenu M. Acquisition, segmentation and tracking of the cerebral vascular tree on 3D magnetic resonance angiography images. *Med Image Anal*. 2001;5(3):173-183. doi:10.1016/S1361-8415(01)00038-X.

81. Hassouna MS, Farag AA, Hushek S, Moriarty T. Cerebrovascular segmentation from TOF using stochastic models. *Med Image Anal*. 2006;10(1):2-18. doi:10.1016/j.media.2004.11.009.

82. Gao X, Uchiyama Y, Zhou X, Hara T, Asano T, Fujita H. A fast and fully automatic method for cerebrovascular segmentation on time-of-flight (TOF) MRA image. *J Digit Imaging*. 2011;24(4):609-625. doi:10.1007/s10278-010-9326-1.

83. Passat N, Ronse C, Baruthio J, Armspach JP, Maillot C. Magnetic resonance angiography: From anatomical knowledge modeling to vessel segmentation. *Med Image Anal*. 2006;10(2):259-274. doi:10.1016/j.media.2005.11.002.

84. Volkau I, Zheng W, Baimouratov R, Aziz A, Nowinski WL. Geometric modeling of the human normal cerebral arterial system. *IEEE Trans Med Imaging*. 2005;24(4):529-539. doi:10.1109/TMI.2005.845041.

85. Schuchardt F, Schroeder L, Anastasopoulos C, et al. In vivo analysis of physiological 3D blood flow of cerebral veins. *Eur Radiol*. 2015. doi:10.1007/s00330-014-3587-x.

86. van Raamt AF, Appelman APA, Mali WPTM, van der Graaf Y. Arterial blood flow to the brain in patients with vascular disease: the SMART Study. *Radiology*. 2006;240(2):515-521. doi:10.1148/radiol.2402050805.

87. Schnell S, Entezari P, Mahadewia RJ, Malaisrie SC. Improved Semiautomated 4D Flow MRI Analysis in the Aorta in Patients With Congenital Aortic Valve Anomalies Versus Tricuspid Aortic Valves. *J Comput Assist Tomogr*. 2016;40(1):102-108. doi:10.1097/RCT.0000000000000312.IMPROVED.

88. Mura J, Pino AM, Sotelo J, et al. Enhancing the Velocity data from 4D flow MR Images by Reducing its Divergence. *IEEE Trans Med Imaging*. 2016;35(10):1-13. doi:10.1109/TMI.2016.2570010.

89. Hoogeveen RM, Bakker CJG, Viergever MA. MR Phase-Contrast Flow Measurement With Limited Spatial Resolution in Small Vessels : Value of Model-Based Image Analysis. *Magn Reson inMedicine*. 1999;41:520-528.

90. Lagerstrand KM, Lehmann H, Starck G, Vikhoff-Baaz B, Ekholm S, Forssell-Aronsson E. Method to correct for the effects of limited spatial resolution in phase-contrast flow MRI measurements. *Magn Reson Med*. 2002;48(5):883-889. doi:10.1002/mrm.10288.

91. Tang C, Parker DL. Correction of Partial-Volume Effects in Phase-Contrast Flow. *J Magn Reson Imaging*. 1995;(5):175-180.

92. Zarrinkoob L, Ambarki K, Wåhlin A, Birgander R, Eklund A, Malm J. Blood flow distribution in cerebral arteries. *J Cereb Blood Flow Metab*. 2015;35(4):648-654. doi:10.1038/jcbfm.2014.241.

93. Gabbour M, Schnell S, Jarvis K, Robinson JD, Markl M, Rigsby CK. 4-D flow magnetic resonance imaging : blood flow quantification compared to 2-D phase-contrast magnetic resonance imaging and Doppler echocardiography. *Pediatr Radiol*. 2015;45:804-813. doi:10.1007/s00247-014-3246-z.

94. Bidhult SL, Carlsson M, Steding-ehrenborg K, Arheden H, Heiberg E. A new method for vessel segmentation based on a priori input from medical expertise in cine phase-contrast Magnetic Resonance Imaging. *J Cardiovasc Magn Reson*. 2014;16(Suppl 1):P355. doi:10.1186/1532-429X-16-S1-P355.

95. Bouillot P, Delattre BMA, Brina O, et al. 3D Phase Contrast MRI : Partial Volume Correction for Robust Blood Flow Quantification in Small Intracranial Vessels. *Magn Reson Med*. 2018;79(1):129-140. doi:10.1002/mrm.26637.

96. Jiang J, Kokeny P, Ying W, Magnano C, Zivadinov R, Haacke EM. Quantifying Errors in Flow Measurement Using Phase Contrast Magnetic Resonance Imaging: Comparison of Several Boundary Detection Methods. *Magn Reson Imaging*. 2015;33(2):185-193. doi:10.1016/j.mri.2014.10.009.

97. Jack CR, Bernstein MA, Fox NC, et al. The Alzheimer's Disease Neuroimaging Initiative (ADNI): MRI methods. *J Magn Reson Imaging*. 2008;27(4):685-691. doi:10.1002/jmri.21049.

98. Amunts K, Lindner A, Zilles K. The human brain project: neuroscience perspectives and German contributions. *e-Neuroforum*. 2014;5:43-50. doi:10.1007/s13295-014-0058-4.

99. Mohammadi D. ENIGMA: crowdsourcing meets neuroscience. *Lancet Neurol*. 2015;14(5):462-463. doi:10.1016/S1474-4422(15)00005-8.

100. Caligiuri ME, Perrotta P, Augimeri A, Rocca F, Quattrone A, Cherubini A. Automatic Detection of White Matter Hyperintensities in Healthy Aging and Pathology Using Magnetic Resonance Imaging: A Review. *Neuroinformatics*. 2015;13(3):261-276. doi:10.1007/s12021-015-9260-y.

101. Harrigan RL, Plassard AJ, Bryan FW, et al. Disambiguating the optic nerve from the surrounding cerebrospinal fluid: Application to MS-related atrophy. *Magn Reson Med*. 2016;75(1):414-422. doi:10.1002/mrm.25613.

102. Jenkinson M, Bannister P, Brady M, Smith S. Improved Optimization for the Robust and Accurate Linear Registration and Motion Correction of Brain Images. *Neuroimage*. 2002;841:825-841. doi:10.1006/nimg.2002.1132.

103. Nevalainen N, Riklund K, Andersson M, et al. COBRA: A prospective multimodal imaging study of dopamine, brain structure and function, and cognition. *Brain Res*. 2015;1612:83-103. doi:10.1016/j.brainres.2014.09.010.

104. Malm J, Jacobsson J, Birgander R, Eklund A. Reference values for CSF outflow resistance and intracranial pressure in healthy elderly. *Neurology*. 2011;76(10):903-909. doi:10.1212/WNL.0b013e31820f2dd0.

105. Johnson KM, Markl M. Improved SNR in phase contrast velocimetry with five-point balanced flow encoding. *Magn Reson Med*. 2010;63(2):349-355. doi:10.1002/mrm.22202.

106. Palàgyi K, Kuba A. A 3D 6-subiteration thinning algorithm for extracting medial lines. *Pattern Recognit Lett*. 1998;19(7):613-627. doi:10.1016/S0167-8655(98)00031-2.

107. Chen Z, Molloi S. Automatic 3D vascular tree construction in CT angiography. *Comput Med Imaging Graph*. 2003;27(6):469-479. doi:10.1016/S0895-6111(03)00039-9.

108. Heiberg E, Sjögren J, Ugander M, Carlsson M, Engblom H, Arheden H. Design and validation of Segment - freely available software for cardiovascular image analysis. *BMC Med Imaging*. 2010;10(1):1-13.

109. Koo TK, Li MY. A Guideline of Selecting and Reporting Intraclass Correlation Coefficients for Reliability Research. *J Chiropr Med*. 2016;15(2):155-163. doi:10.1016/j.jcm.2016.02.012.

110. Love SA, Marie D, Roth M, et al. The average baboon brain: MRI templates and tissue probability maps from 89 individuals. *Neuroimage*. 2016;13:526-533. doi:10.1016/j.neuroimage.2016.03.018.

111. Klein A, Andersson J, Ardekani B a., et al. Evaluation of 14 nonlinear deformation algorithms applied to human brain MRI registration. *Neuroimage*. 2009;46(3):786-802. doi:10.1016/j.neuroimage.2008.12.037.

112. Kiviniemi V, Kantola JH, Jauhiainen J, Hyvärinen A, Tervonen O. Independent component analysis of nondeterministic fMRI signal sources. *Neuroimage*. 2003;19(2):253-260. doi:10.1016/S1053-8119(03)00097-1.

113. Koerte I, Haberl C, Schmidt M, et al. Inter- and intra-rater reliability of blood and CSF flow quantification by phase-contrast MRI. *J Magn Reson Imaging*. 2013;38(3):655-662. doi:10.1002/jmri.24013.

114. Unterhinninghofen R, Ley S, Ley-Zaporozhan J, et al. Concepts for Visualization of Multidirectional Phase-contrast MRI of the Heart and Large Thoracic Vessels. *Acad Radiol*. 2018;15(3):361-369. doi:10.1016/j.acra.2007.11.012.

115. Zarrinkoob L, Wåhlin A, Ambark K, Birgander R, Eklund A, Malm J. Cerebral blood flow distribution in patients with carotid artery stenosis [Unpublished].

116. Nakagawa K, Serrador JM, Larose SL, Moslehi F, Lipsitz LA, Sorond FA. Autoregulation in the Posterior Circulation Is Altered by the Metabolic State of the Visual Cortex. *Stroke*. 2009;40(6):2062-2068. doi:10.1161/STROKEAHA.108.545285.

117. Correia de Verdier M, Wikström J. Normal ranges and test-retest reproducibility of flow and velocity parameters in intracranial arteries measured with phase-contrast magnetic resonance imaging. *Neuroradiology*. 2016:521-531. doi:10.1007/s00234-016-1661-6.

118. Hsiao A, Alley MT, Massaband P, Herfkens RJ, Chan FP, Vasanawala SS. Improved cardiovascular flow quantification with time-resolved volumetric phase-contrast MRI. *Pediatr Radiol*. 2011;41(6):711-720. doi:10.1007/s00247-010-1932-z.

119. Schrauben EM, Johnson KM, Huston J, et al. Reproducibility of cerebrospinal venous blood flow and vessel anatomy with the use of phase contrast-vastly undersampled isotropic projection reconstruction and contrast-enhanced MRA. *Am J Neuroradiol*. 2014;35:999-1006. doi:10.3174/ajnr.A3779.

120. Wåhlin A, Ambarki K, Hauksson J, Birgander R, Malm J, Eklund A. Phase Contrast MRI Quantification of Pulsatile Volumes of Brain Arteries, Veins, and Cerebrospinal Fluids Compartments: Repeatability and Physiological Interactions. *J Magn Reson Imaging*. 2012;35(5):1055-1062. doi:10.1002/jmri.23527.

121. Kamath S. Observations on the length and diameter of vessels forming the circle of Willis. *J Anat*. 1981;133(3):419-423. http://www.pubmedcentral.nih.gov/articlerender.fcgi?artid=1167613&tool=pmcentrez&rendertype=abstract.

122. Ernst M, Forkert ND, Brehmer L, et al. Prediction of Infarction and Reperfusion in Stroke by Flow- and Volume-Weighted Collateral Signal in MR Angiography. *Am J Neuroradiol*. 2015.

123. Alastruey J, Parker KH, Peiró J, Byrd SM, Sherwin SJ. Modelling the circle of Willis to assess the effects of anatomical variations and occlusions on cerebral flows. *J Biomech*. 2007;40(8):1794-1805. doi:10.1016/j.jbiomech.2006.07.008.

124. Pereira VM, Delattre B, Brina O, Bouillot P, Vargas MI. 4D Flow MRI in Neuroradiology : Techniques and Applications. *Top Magn Reson Imaging*. 2016;25(2):81-87.